Available online at www.sciencedirect.com
ScienceDirect
Comput. Methods Appl. Mech. Engrg. 375 (2021) 113649
Computer methods in applied mechanics and engineering
www.elsevier.com/locate/cma

A virtual element method for the miscible displacement of incompressible fluids in porous media

L. Beirão da Veiga[a], A. Pichler[b,*], G. Vacca[a]

[a] *Dipartimento di Matematica e Applicazioni, Università di Milano-Bicocca, 20125 Milano-Bicocca, Italy*
[b] *Faculty of Mathematics, University of Vienna, 1090 Vienna, Austria*

Received 21 August 2020; received in revised form 6 November 2020; accepted 12 December 2020
Available online 2 January 2021

Abstract

In the present contribution, we construct a virtual element (VE) discretization for the problem of miscible displacement of one incompressible fluid by another, described by a time-dependent coupled system of nonlinear partial differential equations. Our work represents a first study to investigate the premises of virtual element methods (VEM) for complex fluid flow problems. We combine the VEM discretization with a time stepping scheme and develop a complete theoretical analysis of the method under the assumption of a regular solution. The scheme is then tested both on a regular and on a more realistic test case.

Keywords: Virtual element methods; Miscible fluid flow; Porous media; Polygonal meshes

1. Introduction

The virtual element method (VEM) was introduced in [1,2] (see also [3]) as a generalization of the finite element method (FEM) that allows to use general polygonal and polyhedral meshes. Since its recent birth in 2013, VEM enjoyed a rapid growth in the mathematics and engineering communities. Among the large number of papers in the literature, we here cite only [4–16] as representatives, see also the references therein.

In the realm of diffusion problems, virtual elements have been developed for linear model diffusion–convection–reaction equations in primal and mixed forms [1,3,17–21], see also [22,23]. It was soon recognized that the flexibility of VEM in terms of meshing could lead to appealing advantages in the presence of complex geometries, such as for discrete fracture network simulation [24–26] and, more in general, in the presence of fractures in porous 3D media [27,28]. Nevertheless, although in other frameworks (such as solid mechanics) VEM have indeed proven themselves also on tough nonlinear problems, to the best knowledge of the authors, virtual elements have never been developed and tested for more complex diffusion models. Since VEM have indeed been hardly tested (with very promising outcomes) on linear diffusion problems with complex geometries, as often encountered in geophysical flows, developing a VEM also for more complex (and realistic) flow models becomes a key step towards a competitive methodology for applications.

* Corresponding author.
E-mail addresses: lourenco.beirao@unimib.it (L. Beirão da Veiga), alex.pichler@univie.ac.at (A. Pichler), giuseppe.vacca@unimib.it (G. Vacca).

https://doi.org/10.1016/j.cma.2020.113649

In the present contribution, we consider the miscible displacement of one incompressible fluid by another in a reservoir, described by a time-dependent coupled system of nonlinear partial differential equations, that is a basic (but meaningful) model instrumental to applications such as oil recovery and environmental pollution [29–35]. One must note that, on this and similar models, there already exists a large literature with many competitive schemes, adopting for instance finite elements [31,36–38], discontinuous Galerkin methods [39–44], and finite volumes [32,45,46] and also other more recent polytopal technologies [47–49]. The aim of the present paper is to make a first study on the premises of VEM in this framework (by proposing a numerical scheme, giving a theoretical backbone to it, and finally testing it numerically). Incompressible miscible displacements in porous media arising from geophysical real-life problem may pose severe constraints to the creation of the computational grids, since their geometry may give rise to distorted and badly shaped grid elements. We believe that the VEM is suited for such kind of mesh complexity. Indeed, it can handle arbitrary shaped polygons, it is robust with respect to the mesh features and to element distortion. Moreover the proposed VEM discretization produces conforming velocity/concentration solutions, that is an important difference with respect to other competitive polytopal technologies, such as for instance the discontinuous Galerkin methods.

From the mathematical viewpoint, the above model yields a nonlinear time-dependent coupled problem for concentration, velocity and pressure, also with potential issues of stability (at the discrete level) due to possible convection-dominated regimes. We propose a continuous (H^1 conforming) approximation for the concentration variable, thus leading to nodal virtual elements [1,17], and an $H(\mathrm{div})$ conforming approximation of the Darcy velocity, thus leading to face virtual elements [18,50]. For the pressure, we adopt a standard piecewise discontinuous polynomial space. Due to the presence of the non-linear coefficients coupling the two set of equations, we make use of projection operators to approximate such terms and of stabilization factors that are suitably chosen. We combine the VEM discretization in space with a simple discretization procedure in time, that is a backward Euler approximation that is explicit in the coefficient terms. As a consequence, the system to be solved at each time step is linear and decoupled, leading to a cheap procedure. Extending the proposed scheme to different time discretization procedures would be, on the basis of the work presented here, quite trivial.

After proposing the method, we develop an error analysis under the assumption of a regular solution. Although such regularity conditions are unrealistic in most cases of interest, we believe that the derived results are still critical in order to give a theoretical backbone to the method. They serve the purpose of showing that the method indeed delivers a solution with the potential to yield the correct approximation order whenever this is feasible (given the approximability of the target solution by the discrete space). No time step size condition is needed in the analysis. Finally, we test the proposed scheme in three different ways. We firstly consider a problem with known regular solution inspired from [51], in order to validate the convergence properties of the method also in practice and to test some other practical aspect such as the possibility of having different time step sizes for the two different equations. In the second test, we show the potential of the "local refinement" that one can achieve with VEM, in particular, we assess the robustness of the VEM technology in presence of meshes with many hanging nodes and edges with different size. Then, we consider a more realistic test, taken from [52], in order to have a qualitative comparison with the expected benchmark solution from the literature. In this third test, there is also the risk of overshoots and undershoots in the discrete solution due to strong convection. We here deal with this aspect by introducing in our scheme a modification borrowed from [53], that is recognized in [54] to be one of the best choices in practice. From the present first theoretical and numerical studies, we believe the VEM is promising and has the possibility to become, after further developments, a competitive scheme for complex flow problems.

The structure of the paper is the following: In Section 2, we introduce the continuous problem, in strong and weak forms. In Section 3, we describe the proposed virtual element discretization, in space and time. In Section 4, we develop the theoretical convergence analysis of the scheme. In Section 5, we show the numerical results. Finally, in the Appendix, we briefly describe the extension of the method to the three-dimensional case.

2. Problem description

We consider the miscible displacement of one incompressible fluid by another in a porous medium. This problem can be formulated in terms of a system of partial differential equations, where a parabolic diffusion–convection–reaction type equation is nonlinearly coupled with an elliptic system, see also [30–33].

We need to introduce some notation and conventions to be adopted throughout the paper. We denote by $\mathbb{N}$ and $\mathbb{N}_0$ the sets of all natural numbers without and including zero, respectively. Moreover, we employ the standard

notation for Sobolev spaces, norms, and seminorms. More precisely, for a given bounded Lipschitz domain $D \subset \mathbb{R}^2$, $k \in \mathbb{N} \cup \{\infty\}$, and $p \in \mathbb{N}$, we define by $W^{k,p}(D)$ the space of all L^p integrable functions over D whose weak derivatives up to order k are again L^p integrable. Sobolev spaces with fractional order can be defined for instance via interpolation theory [55]. For $p = 2$, we write $H^k(D) \coloneqq W^{k,2}(D)$, and we use $(\cdot,\cdot)_{k,D}$, $|\cdot|_{k,D}$, and $\|\cdot\|_{k,D}$, to denote the corresponding inner product, seminorm, and norm, respectively. The standard L^2 inner product over D is written as $(\cdot,\cdot)_{0,D}$ with corresponding norm $\|\cdot\|_{0,\Omega}$. Further, $\mathbb{P}_k(D)$ is the space of polynomials up to order k, and $[\mathbb{P}_k(D)]^2$ the corresponding vector valued space. Additionally, $|\cdot|$ is the standard Euclidean norm for scalars and vectors. Finally, throughout the paper, η denotes a generic constant, possibly varying from one occurrence to the other, but independent of the mesh size and, apart from Theorem 2, also independent of the variables.

2.1. Continuous problem

Let $\Omega \subset \mathbb{R}^2$ be a polygonal bounded, convex domain, describing a reservoir of unit thickness. Given a time interval $J \coloneqq [0, T]$, for $T > 0$, we are interested in finding $\boldsymbol{u} = \boldsymbol{u}(\boldsymbol{x}, t)$, representing the Darcy velocity (volume of fluid flowing cross a unit across-section per unit time), the pressure $p = p(\boldsymbol{x}, t)$ in the fluid mixture (that we assume having zero mean value), and the concentration $c = c(\boldsymbol{x}, t)$ of one of the fluids (amount of the fluid per unit volume in the fluid mixture), with $(\boldsymbol{x}, t) \in \Omega_T \coloneqq \Omega \times J$, such that

$$\begin{cases} \phi \dfrac{\partial c}{\partial t} + \boldsymbol{u} \cdot \nabla c - \operatorname{div}(D(\boldsymbol{u})\nabla c) = q^+(\widehat{c} - c) \\ \qquad\qquad \operatorname{div} \boldsymbol{u} = G \\ \qquad\qquad \boldsymbol{u} = -a(c)(\nabla p - \boldsymbol{\gamma}(c)), \end{cases} \tag{1}$$

where $\phi = \phi(\boldsymbol{x})$ is the porosity of the medium, $q^+ = q^+(\boldsymbol{x}, t)$ and $q^- = q^-(\boldsymbol{x}, t)$ are the (non negative) injection and production source terms, respectively, $\widehat{c} = \widehat{c}(\boldsymbol{x}, t)$ is the concentration of the injected fluid, and

$$G \coloneqq q^+ - q^-. \tag{2}$$

Moreover, $D(\boldsymbol{u}) \in \mathbb{R}^{2\times 2}$ is the diffusion tensor given by

$$D(\boldsymbol{u}) \coloneqq \phi \left[d_m I + |\boldsymbol{u}|(d_\ell E(\boldsymbol{u}) + d_t E^\perp(\boldsymbol{u})) \right], \tag{3}$$

with matrices

$$E(\boldsymbol{u}) \coloneqq \left(\frac{\boldsymbol{u}_i \boldsymbol{u}_j}{|\boldsymbol{u}|^2} \right)_{i,j=1,2} = \frac{\boldsymbol{u}\boldsymbol{u}^T}{|\boldsymbol{u}|^2}, \quad E^\perp(\boldsymbol{u}) \coloneqq I - E(\boldsymbol{u}),$$

and molecular diffusion coefficient d_m, longitudinal dispersion coefficient d_ℓ, and transversal dispersion coefficient d_t. Further, $\boldsymbol{\gamma}(c)$ in (1) describes the force density due to gravity (typically written as $\boldsymbol{\gamma}(c) = \gamma_0(c)\boldsymbol{\rho}$ with $\gamma_0(c)$ being the density of the fluid and $\boldsymbol{\rho}$ the gravitational acceleration vector), and $a(c) = a(c, \boldsymbol{x})$ is the scalar valued function given by

$$a(c) \coloneqq \frac{k}{\mu(c)},$$

where $k = k(\boldsymbol{x})$ represents the permeability of the porous rock, and $\mu(c)$ is the viscosity of the fluid mixture, which can be modeled by

$$\mu(c) = \mu(0) \left(1 + \left(M^{\frac{1}{4}} - 1 \right) c \right)^{-4}, \quad \text{in } [0, 1],$$

with mobility ratio $M \coloneqq \frac{\mu(0)}{\mu(1)}$. Note that μ can be set to $\mu(0)$ for $c < 0$, and to $\mu(1)$ for $c > 1$. We also highlight that, in the literature, k is sometimes assumed to be a tensor. The following analysis can be straightforwardly generalized to that case.

Assuming impermeability of $\partial\Omega$, the system (1) is closed by requiring *no-flow boundary conditions* of the form

$$\begin{cases} \boldsymbol{u} \cdot \boldsymbol{n} = 0 & \text{on } \partial\Omega \times J \\ D(\boldsymbol{u})\nabla c \cdot \boldsymbol{n} = 0 & \text{on } \partial\Omega \times J, \end{cases} \tag{4}$$

and initial condition

$$c(\boldsymbol{x}, 0) = c_0(\boldsymbol{x}) \quad \text{in } \Omega, \tag{5}$$

where $0 \leq c_0(\boldsymbol{x}) \leq 1$ is an initial concentration.

By use of the divergence theorem, the boundary conditions (4) directly imply the following compatibility condition for q^+ and q^-:

$$\int_\Omega q^+(\boldsymbol{x}, t)\,\mathrm{d}x = \int_\Omega q^-(\boldsymbol{x}, t)\,\mathrm{d}x,$$

for every $t \in J$.

We highlight that, in the forthcoming theoretical analysis, we will always assume sufficient regularity of the exact solution and the involved functions, such as q^+, q^-, $\widehat{c}$, *et cetera*, as better motivated in the corresponding section. Moreover, we will make use of the following assumptions.

First of all, we suppose that the functions a and ϕ are positive and uniformly bounded from below and above, i.e. there exist positive constants a_*, a^*, ϕ_*, and ϕ^*, such that

$$a_* \leq a(z, \boldsymbol{x}) \leq a^*, \qquad \phi_* \leq \phi(\boldsymbol{x}) \leq \phi^*, \tag{6}$$

for all $\boldsymbol{x} \in \Omega$ and $z = z(t)$. For the sake of readability, we define

$$A(z)(\boldsymbol{x}) := a^{-1}(z, \boldsymbol{x}).$$

Additionally, we will make use of the following relation of the diffusion and dispersion coefficients, which was observed in laboratory experiments:

$$0 < d_m \leq d_t \leq d_\ell. \tag{7}$$

Finally, we recall that the source terms q^+ and q^- are, as usual, assumed to be non-negative functions.

Existence of weak solutions to this model problem was shown in [56] for $\boldsymbol{\gamma}(c) = 0$. An extension of this result to 3D spatial domains, including the presence of $\boldsymbol{\gamma}(c)$ and various boundary conditions was discussed in [57].

2.2. Weak formulation of the continuous problem

Here, we fix the basic notation and the functional setting.

To this purpose, given Ω as above, we first introduce the Sobolev space

$$H(\mathrm{div};\, \Omega) := \{\boldsymbol{v} \in [L^2(\Omega)]^2 :\ \mathrm{div}\, \boldsymbol{v} \in L^2(\Omega)\}.$$

Then, we define the velocity space $\boldsymbol{V}$, the pressure space Q, and the concentration space Z by

$$\begin{aligned} \boldsymbol{V} &:= \{\boldsymbol{v} \in H(\mathrm{div};\, \Omega) :\ \boldsymbol{v} \cdot \boldsymbol{n} = 0 \ \text{ on } \partial\Omega\} \\ Q &:= L^2_0(\Omega) := \{\varphi \in L^2(\Omega) :\ (\varphi, 1)_{0,\Omega} = 0\} \\ Z &:= H^1(\Omega), \end{aligned} \tag{8}$$

respectively. These spaces are endowed, respectively, with the following norms:

$$\|\boldsymbol{u}\|^2_{\boldsymbol{V}} := \|\boldsymbol{u}\|^2_{0,\Omega} + \|\,\mathrm{div}\, \boldsymbol{u}\|^2_{0,\Omega}, \qquad \|q\|^2_Q := \|q\|^2_{0,\Omega}, \qquad \|z\|^2_Z := \|z\|^2_{1,\Omega} := \|\nabla z\|^2_{0,\Omega} + \|z\|^2_{0,\Omega}.$$

Note that $\mathrm{div}\, \boldsymbol{V} = Q$.

As usual in the framework of parabolic problems, we use the notation

$$\boldsymbol{u}(t)(x) := \boldsymbol{u}(x, t), \qquad p(t)(x) := p(x, t), \qquad c(t)(x) := c(x, t). \tag{9}$$

For $0 \leq a \leq b$, we further introduce

$$\|\boldsymbol{v}\|_{L^2(a,b;\boldsymbol{V})} := \left(\int_a^b \|\boldsymbol{v}(t)\|^2_{\boldsymbol{V}}\,\mathrm{d}x\right)^{\frac{1}{2}}, \quad \|\boldsymbol{v}\|_{L^\infty(a,b;\boldsymbol{V})} := \operatorname*{ess\,sup}_{t\in[a,b]} \|\boldsymbol{v}(t)\|_{\boldsymbol{V}};$$

analogously for p and c.

Having this, the continuous problem reads as follows: find $c \in L^2(0,T;Z)\cap C^0([0,T];L^2(\Omega))$, $\boldsymbol{u} \in L^2(0,T;\boldsymbol{V})$, and $p \in L^2(0,T;Q)$, such that

$$\begin{cases} \mathcal{M}\left(\dfrac{\partial c(t)}{\partial t}, z\right) + (\boldsymbol{u}(t)\cdot\nabla c(t), z)_{0,\Omega} + \mathcal{D}(\boldsymbol{u}(t);c(t),z) = \left(q^+(\widehat{c}-c)(t), z\right)_{0,\Omega} \\ \mathcal{A}(c(t);\boldsymbol{u}(t),\boldsymbol{v}) + B(\boldsymbol{v},p(t)) = (\boldsymbol{\gamma}(c(t)),\boldsymbol{v})_{0,\Omega} \\ B(\boldsymbol{u}(t),q) = -(G(t),q)_{0,\Omega} \end{cases} \tag{10}$$

for all $\boldsymbol{v} \in \boldsymbol{V}$, $q \in Q$, and $z \in Z$, for almost all $t \in J$ and with initial condition $c(0) = c_0$, where

$$\begin{aligned} \mathcal{M}(c,z) &:= (\phi\, c, z)_{0,\Omega}\,, & \mathcal{D}(\boldsymbol{u};c,z) &:= (D(\boldsymbol{u})\nabla c, \nabla z)_{0,\Omega}\,, \\ \mathcal{A}(c;\boldsymbol{u},\boldsymbol{v}) &:= (A(c)\boldsymbol{u},\boldsymbol{v})_{0,\Omega}\,, & B(\boldsymbol{v},q) &:= -(\operatorname{div}\boldsymbol{v},q)_{0,\Omega}\,. \end{aligned} \tag{11}$$

Note that $c \in L^2(0,T;Z)\cap C^0([0,T];L^2(\Omega))$ implies $\frac{\partial c}{\partial t} \in L^2(0,T;Z')$, see e.g. [58, Thm. 11.1.1].

For the sake of readability, we suppressed (t) in (11). From now on, we will use the convention that by writing $\boldsymbol{u}$, we mean in fact $\boldsymbol{u}(t)$; similarly for the other functions depending on space and time. In general it will be clear from the context whether $\boldsymbol{u}$ represents $\boldsymbol{u}(t)$ for a fixed $t \in J$, i.e. as a function of space only, or for varying $\boldsymbol{x}$ and t, as a function of both space and time.

Moreover, we will use the following alternative form for the concentration equation:

$$\mathcal{M}\left(\frac{\partial c}{\partial t}, z\right) + \Theta(\boldsymbol{u},c;z) + \mathcal{D}(\boldsymbol{u};c,z) = \left(q^+\widehat{c}, z\right)_{0,\Omega}\,, \tag{12}$$

where

$$\Theta(\boldsymbol{u},c;z) := \frac{1}{2}\Big[(\boldsymbol{u}\cdot\nabla c, z)_{0,\Omega} + ((q^+ + q^-)\,c, z)_{0,\Omega} - (\boldsymbol{u}, c\,\nabla z)_{0,\Omega}\Big].$$

This version is obtained from the original one in (10) by rewriting the convective term as

$$(\boldsymbol{u}\cdot\nabla c, z)_{0,\Omega} = \frac{1}{2}\big[(\boldsymbol{u}\cdot\nabla c, z)_{0,\Omega} - (G, c\,z)_{0,\Omega} - (\boldsymbol{u}, c\,\nabla z)_{0,\Omega}\big],$$

where we first integrated by parts, then employed the fact that $\nabla\cdot\boldsymbol{u} = G$, together with the definition of G in (2), and afterwards combined this term with $(q^+ c, z)_{0,\Omega}$ from the right hand side of (10). This representation was inspired by the theory of VEM for general elliptic problems [6] and helps to ensure that properties of the continuous bilinear will be preserved after discretization.

In the rest of this section, we summarize some properties of the forms $\mathcal{M}(\cdot,\cdot)$, $\mathcal{A}(\cdot,\cdot,\cdot)$ and $\mathcal{D}(\cdot;\cdot,\cdot)$, all defined in (11), which will be needed later on.

To start with, for $\mathcal{M}(\cdot,\cdot)$, it directly holds with the Cauchy–Schwarz inequality and (6)

$$\mathcal{M}(c,z) \le \phi^*\|c\|_{0,\Omega}\|z\|_{0,\Omega}, \qquad \mathcal{M}(z,z) \ge \phi_*\|z\|^2_{0,\Omega},$$

for all $c, z \in Z$.

Concerning $\mathcal{A}(\cdot;\cdot,\cdot)$, again employing (6), for all $c \in L^\infty(\Omega)$ and $\boldsymbol{u},\boldsymbol{v} \in [L^2(\Omega)]^2$, we have

$$\mathcal{A}(c;\boldsymbol{u},\boldsymbol{v}) \le \frac{1}{a_*}\|\boldsymbol{u}\|_{0,\Omega}\|\boldsymbol{v}\|_{0,\Omega}.$$

Further, if $c \in L^2(\Omega)$, $\boldsymbol{u} \in [L^\infty(\Omega)]^2$ and $\boldsymbol{v} \in [L^2(\Omega)]^2$, it holds true that

$$\mathcal{A}(c;\boldsymbol{u},\boldsymbol{v}) \le \|A(c)\|_{0,\Omega}\|\boldsymbol{u}\|_{\infty,\Omega}\|\boldsymbol{v}\|_{0,\Omega}.$$

We also have the coercivity bound

$$\mathcal{A}(c;\boldsymbol{v},\boldsymbol{v}) \ge \frac{1}{a^*}\|\boldsymbol{v}\|^2_{0,\Omega}$$

for all $c \in L^\infty(\Omega)$ and $\boldsymbol{v} \in [L^2(\Omega)]^2$, from which, after defining the kernel

$$\mathcal{K} := \{\boldsymbol{v} \in \boldsymbol{V} :\ B(\boldsymbol{v},q) = 0 \quad \forall q \in Q\}, \tag{13}$$

coercivity of $\mathcal{A}(c;\cdot,\cdot)$ on $\mathcal{K}$ in the norm $\|\cdot\|_V$ follows.

Regarding $\mathcal{D}(\cdot;\cdot,\cdot)$, the following continuity properties can be shown. Firstly, for all $\boldsymbol{u} \in [L^\infty(\Omega)]^2$ and $c, z \in H^1(\Omega)$, we have

$$\mathcal{D}(\boldsymbol{u}; c, z) \leq \phi^* \left[d_m + \|\boldsymbol{u}\|_{\infty,\Omega}(d_\ell + d_t)\right] \|\nabla c\|_{0,\Omega} \|\nabla z\|_{0,\Omega}, \tag{14}$$

which follows directly from the Cauchy–Schwarz inequality, the definition of $D(\boldsymbol{u})$ in (3), and the fact that $|E(\boldsymbol{u})\boldsymbol{v}| \leq |\boldsymbol{v}|$ and $|E^\perp(\boldsymbol{u})\boldsymbol{v}| \leq |\boldsymbol{v}|$ for all $\boldsymbol{v} \in \mathbb{R}^2$. Moreover, for all $\boldsymbol{u} \in [L^2(\Omega)]^2$ and $c, z \in H^1(\Omega)$ with $\nabla c \in L^\infty(\Omega)$, we have the bound

$$\mathcal{D}(\boldsymbol{u}; c, z) \leq \|D(\boldsymbol{u})\|_{0,\Omega} \|\nabla c\|_{\infty,\Omega} \|\nabla z\|_{0,\Omega} \leq \eta_{\mathcal{D}}(1 + \|\boldsymbol{u}\|_{0,\Omega}) \|\nabla c\|_{\infty,\Omega} \|\nabla z\|_{0,\Omega}, \tag{15}$$

with matrix norm $\|D(\boldsymbol{u})\|_{0,\Omega} := \left(\sum_{i,j=1}^2 \|D_{i,j}(\boldsymbol{u})\|_{0,\Omega}^2\right)^{\frac{1}{2}}$, and some positive constant $\eta_{\mathcal{D}}$ depending only on d_m, d_ℓ, and d_t. In addition, coercivity of $\mathcal{D}(\boldsymbol{u};\cdot,\cdot)$ for all $\boldsymbol{u} \in [L^\infty(\Omega)]^2$, with respect to $\|\cdot\|_{0,\Omega}$, follows from

$$\begin{aligned}(D(\boldsymbol{u})\,\boldsymbol{\mu}, \boldsymbol{\mu})_{0,\Omega} &= (\phi\, d_m\, \boldsymbol{\mu}, \boldsymbol{\mu})_{0,\Omega} + (\phi\, |\boldsymbol{u}|\, (d_\ell E(\boldsymbol{u}) + d_t E^\perp(\boldsymbol{u}))\, \boldsymbol{\mu}, \boldsymbol{\mu})_{0,\Omega} \\ &\geq \phi_*\, d_m\, \|\boldsymbol{\mu}\|_{0,\Omega}^2 + (\phi\, |\boldsymbol{u}|(d_\ell - d_t)E(\boldsymbol{u})\boldsymbol{\mu}, \boldsymbol{\mu})_{0,\Omega} + (\phi\, |\boldsymbol{u}| d_t\, \boldsymbol{\mu}, \boldsymbol{\mu})_{0,\Omega} \\ &\geq \phi_* \left(d_m\, \|\boldsymbol{\mu}\|_{0,\Omega}^2 + d_t\, \||\boldsymbol{u}|^{\frac{1}{2}} \boldsymbol{\mu}\|_{0,\Omega}^2\right)\end{aligned} \tag{16}$$

for all $\boldsymbol{\mu} \in [L^2(\Omega)]^2$, where we also employed (6) and (7).

3. The virtual element method

In this section, we derive a virtual element formulation for the model problem (10). To this purpose, we firstly fix the concept of polygonal decompositions of Ω in Section 3.1, and then, we introduce a set of discrete spaces, discrete bilinear forms, and projectors in Section 3.2. Having these ingredients, we state a semidiscrete formulation which is continuous in time and discrete in space in Section 3.3. The fully discrete formulation is the subject of Section 3.4.

3.1. Polygonal decompositions

Let $\mathcal{T}_h$ be a discretization of Ω into polygons K. We denote by $\mathcal{E}_h$ the set of all edges of $\mathcal{T}_h$, and, for a given element $K \in \mathcal{T}_h$, by $\mathcal{E}^K$ the set of edges belonging to K. Furthermore, n_K is the number of edges of K, h_K is the diameter of K, and $h := \max_{K\in\mathcal{T}_h} h_K$. For a given edge $e \in \mathcal{E}_h$, we write h_e for its length. Having this, we make the following assumptions on $\mathcal{T}_h$: there exists $\rho_0 > 0$ such that, for all $h > 0$ and for all $K \in \mathcal{T}_h$,

(**D1**) K is star-shaped with respect to a ball of radius $\rho \geq \rho_0 h_K$;
(**D2**) $h_e \geq \rho_0 h_K$ for all $e \in \mathcal{E}^K$.

Note that these two assumptions imply that the number of edges of each element is uniformly bounded. Additionally, we will require quasi-uniformity:

(**D3**) for all $h > 0$ and for all $K \in \mathcal{T}_h$, it holds $h_K \geq \rho_1 h$, for some positive uniform constant ρ_1.

Given $\mathcal{T}_h$, we define, for all $s > 0$, the broken Sobolev spaces on $\mathcal{T}_h$ as

$$H^s(\mathcal{T}_h) := \{v \in L^2(\Omega) \mid v_{|_K} \in H^s(K)\ \forall K \in \mathcal{T}_h\},$$

together with the corresponding broken seminorms and norms

$$|v|_{s,\mathcal{T}_h}^2 := \sum_{K\in\mathcal{T}_h} |v|_{s,K}^2, \qquad \|v\|_{s,\mathcal{T}_h}^2 := \sum_{K\in\mathcal{T}_h} \|v\|_{s,K}^2. \tag{17}$$

Remark 3.1. Both assumptions (**D1**) and (**D2**) are standard in the virtual element literature. While condition (**D1**) is quite critical in the following analysis, assumption (**D2**) could be possibly avoided by following steps similar to [59–61], at the expense of making the proofs even more lengthy and technical. Finally, assumption (**D3**) (that can be found also in many FEM papers on the same subject) is only needed to prove bound (62).

3.2. Discrete spaces and projectors

Here, we introduce the local discrete VE spaces corresponding to $\boldsymbol{V}$, Q and Z in (8), a set of local projectors mapping from these VE spaces into spaces made of polynomials, and finally, the related global counterparts.

3.2.1. Local discrete spaces

Let $K \in \mathcal{T}_h$ and let $k \in \mathbb{N}_0$ be a given *degree of accuracy*. Then, the local velocity and pressure VE spaces are defined by [18,62]

$$\begin{aligned} \boldsymbol{V}_h(K) &:= \{\boldsymbol{v} \in H(\mathrm{div};K) \cap H(\mathrm{rot};K) : \boldsymbol{v}\cdot\boldsymbol{n}_{|_e} \in \mathbb{P}_k(e)\,\forall e \in \mathcal{E}^K, \\ &\qquad \mathrm{div}\,\boldsymbol{v} \in \mathbb{P}_k(K),\ \mathrm{rot}\,\boldsymbol{v} \in \mathbb{P}_{k-1}(K)\} \\ Q_h(K) &:= \{q \in L^2(K) : q \in \mathbb{P}_k(K)\}. \end{aligned} \tag{18}$$

These spaces are coupled with the *preliminary* local concentration space

$$\widetilde{Z}_h(K) := \{z \in H^1(K) : z_{|_{\partial K}} \in C^0(\partial K),\ z_{|_e} \in \mathbb{P}_{k+1}(e)\,\forall e \in \mathcal{E}^K,\ \Delta z \in \mathbb{P}_{k-1}(K)\}. \tag{19}$$

Moreover, it is important to observe that $[\mathbb{P}_k(K)]^2 \subset \boldsymbol{V}_h(K)$ and $\mathbb{P}_{k+1}(K) \subseteq \widetilde{Z}_h(K)$. Associated sets of local degrees of freedom are given as follows:

- for $\boldsymbol{V}_h(K)$, a set of degrees of freedom $\{\mathrm{dof}_j^{\boldsymbol{V}_h(K)}\}_{j=1}^{\dim \boldsymbol{V}_h(K)}$ is defined by

$$\begin{aligned} &1.\quad \frac{1}{|e|}\int_e \boldsymbol{v}\cdot\boldsymbol{n}\, p_k\,\mathrm{d}s \qquad \forall p_k \in \mathbb{P}_k(e) \quad \forall e \in \mathcal{E}^K \\ &2.\quad \frac{1}{|K|^{\frac{1}{2}}}\int_K (\mathrm{div}\,\boldsymbol{v})\, p_k\,\mathrm{d}x \qquad \forall p_k \in \mathbb{P}_k(K)/\mathbb{R} \\ &3.\quad \frac{1}{|K|}\int_K \boldsymbol{v}\cdot\boldsymbol{x}^\perp\, p_{k-1}\,\mathrm{d}x \qquad \forall p_{k-1} \in \mathbb{P}_{k-1}(K), \end{aligned} \tag{20}$$

  with $\boldsymbol{x}^\perp := (x_2, -x_1)^T$, where we assume the coordinates to be centered at the barycenter of the element;
- for $Q_h(K)$, we consider $\{\mathrm{dof}_j^{Q_h(K)}\}_{j=1}^{\dim Q_h(K)}$ with

$$\frac{1}{|K|}\int_K q\, p_k\,\mathrm{d}x \qquad \forall p_k \in \mathbb{P}_k(K); \tag{21}$$

- for $\widetilde{Z}_h(K)$, we take $\{\mathrm{dof}_j^{\widetilde{Z}_h(K)}\}_{j=1}^{\dim \widetilde{Z}_h(K)}$ with

$$\begin{aligned} &1.\quad \text{pointwise values at the vertices: } z(\boldsymbol{v}) \\ &2.\quad \text{on each edge } e \in \mathcal{E}^K, \text{ the values of } z \text{ at the } k \text{ internal Gauß–Lobatto points} \\ &3.\quad \frac{1}{|K|}\int_K z\, q_{k-1}\,\mathrm{d}x \qquad \forall q_{k-1} \in \mathbb{P}_{k-1}(K). \end{aligned} \tag{22}$$

In all three cases, unisolvency is provided. More precisely, for $\boldsymbol{V}_h(K)$, this was proven in e.g. [62], for $Q_h(K)$ it is immediate, and for $\widetilde{Z}_h(K)$, see e.g. [1].

Notice that the discrete velocities and the discrete concentrations (cf. (18) and (19) respectively) are not known in closed form but are defined implicitly as the solutions of suitable PDEs inside the polygon. We recall that on a simple polygon K both systems of differential equations are well posed (assuming the compatibility of the boundary and the divergence data). We also highlight that $\boldsymbol{V}_h(K)$ endowed with (20) mimics the Raviart–Thomas element, but in fact those two elements only coincide in the special case of triangles and $k = 0$. Analogously the lowest order version of $\widetilde{Z}_h(K)$ coincides with the standard $\mathbb{P}_1$ (resp. $\mathbb{Q}_1$) on triangles (resp. quads).

Remark 3.2. We note that, for $k = 0$, one obtains the lowest order local VE spaces. More precisely, in this case, the velocity space $\boldsymbol{V}_h(K)$ consists of all rotation-free vector fields with constant divergence and edgewise constant normal traces, the pressure space $Q_h(K)$ only contains the constant functions, and the concentration space $\widetilde{Z}_h(K)$ is made of all harmonic functions that are linear on each edge. This motivates the choice of the present polynomial degrees for the spaces. However, in general, it is also possible to choose a degree of accuracy k_1 for

$\boldsymbol{V}_h(K)$ and $Q_h(K)$, and another strictly positive one k_2 for $\widetilde{Z}_h(K)$; see e.g. [31] for FEM. The following analysis can be extended easily to such more general case just by keeping track of the different polynomial degrees.

Remark 3.3. In order to really have a set of degrees of freedom in the computer code, one clearly needs to choose a basis for the polynomial test spaces appearing in (20) and (22). We here assume to take the classical choice, that is any monomial basis $\{m_1, m_2, \dots, m_\ell\}$ of the polynomial space satisfying $\|m_i\|_{L^\infty} \simeq 1$, $i = 1, 2, \dots, \ell$, where the L^∞ norm has to be taken over the corresponding edge or bulk.

3.2.2. Local projections

For the construction of the method, we will need some tools to deal with VE functions due to the lack of their explicit knowledge in closed form. These tools will be provided in the form of local operators mapping VE functions onto polynomials. To this purpose, following [1,2], we introduce the subsequent projectors.

The projector $\boldsymbol{\Pi}_k^{\mathbf{0},K} : [L^2(K)]^2 \to [\mathbb{P}_k(K)]^2$ is defined as the L^2 projector onto vector valued polynomials of degree at most k in each component: Given $\boldsymbol{f} \in [L^2(\Omega)]^2$,

$$(\boldsymbol{\Pi}_k^{\mathbf{0},K} \boldsymbol{f}, \boldsymbol{p}_k)_{0,K} = (\boldsymbol{f}, \boldsymbol{p}_k)_{0,K} \quad \forall \boldsymbol{p}_k \in [\mathbb{P}_k(K)]^2. \tag{23}$$

It can be shown, see [17], that this operator is computable for functions in $\boldsymbol{V}_h(K)$ only by knowing their values at the degrees of freedom (20). Moreover, one has computability also for functions of the form ∇z_h with $z_h \in \widetilde{Z}_h(K)$. This can be seen by using integration by parts:

$$\int_K (\boldsymbol{\Pi}_k^{\mathbf{0},K} \nabla z_h) \cdot \boldsymbol{p}_k \, \mathrm{d}s = \int_K \nabla z_h \cdot \boldsymbol{p}_k \, \mathrm{d}s = -\int_K z_h \underbrace{\operatorname{div} \boldsymbol{p}_k}_{\in \mathbb{P}_{k-1}(K)} \, \mathrm{d}s + \int_{\partial K} z_h \, \boldsymbol{p}_k \cdot \boldsymbol{n} \, \mathrm{d}s,$$

for all $\boldsymbol{p}_k \in [\mathbb{P}_k(K)]^2$, where the right hand side is computable by means of (22).

The projector $\Pi_{k+1}^{\nabla,K} : H^1(K) \to \mathbb{P}_{k+1}(K)$ is given, for every $z \in H^1(K)$, by

$$\begin{cases} (\nabla \Pi_{k+1}^{\nabla,K} z, \nabla p_k)_{0,K} = (\nabla z, \nabla p_k)_{0,K} \quad \forall p_{k+1} \in \mathbb{P}_{k+1}(K) \\ \dfrac{1}{|\partial K|} \displaystyle\int_{\partial K} \Pi_{k+1}^{\nabla,K} z \, \mathrm{d}s = \dfrac{1}{|\partial K|} \int_{\partial K} z \, \mathrm{d}s, \end{cases}$$

where the second identity is needed to fix the constants. Computability of this mapping for functions in $\widetilde{Z}_h(K)$ was shown in [1,2].

3.2.3. Discrete space for concentrations

The space introduced in (19) was a preliminary space, useful to introduce the main idea of the construction. Nevertheless, we will here make use of a more advanced space for the discrete concentration variable. Indeed, one can use the operator $\Pi_{k+1}^{\nabla,K}$ to pinpoint the local enhanced space

$$Z_h(K) := \{z \in H^1(K) : z_{|\partial K} \in C^0(\partial K),\ z_{|e} \in \mathbb{P}_{k+1}(e) \forall e \in \mathcal{E}^K,\ \Delta z \in \mathbb{P}_{k+1}(K),$$
$$\int_K z \, p_k \, \mathrm{d}x = \int_K (\Pi_{k+1}^{\nabla,K} z) \, p_k \, \mathrm{d}x \quad \forall p_k \in \mathbb{P}_{k+1}/\mathbb{P}_{k-1}(K)\},$$

where $\mathbb{P}_{k+1}/\mathbb{P}_{k-1}(K)$ is the space of polynomials in $\mathbb{P}_{k+1}(K)$ which are $L^2(K)$ orthogonal to $\mathbb{P}_{k-1}(K)$. It can be shown that the space $Z_h(K)$ has the same dimension and the same degrees of freedom (22) as $\widetilde{Z}_h(K)$, see [63,64]. The advantage of the space $Z_h(K)$, when compared to $\widetilde{Z}_h(K)$, is that *also* the L^2 projector $\Pi_{k+1}^{0,K} : L^2(K) \to \mathbb{P}_{k+1}(K)$ onto polynomials of degree at most $k+1$, defined analogously to (23), is computable [2]

Finally, we state the following approximation result for the three projectors above [17, Lemma 5.1]:

Lemma 3.1. *Given $K \in \mathcal{T}_h$, let ψ and $\boldsymbol{\psi}$ be sufficiently smooth scalar and vector valued functions, respectively. Then, it holds, for all $k \in \mathbb{N}_0$,*

$$\|\psi - \Pi_k^{0,K} \psi\|_{\ell,K} \le \zeta \, h_K^{s-\ell} \, |\psi|_{s,K}, \quad 0 \le \ell \le s \le k+1$$
$$\|\boldsymbol{\psi} - \boldsymbol{\Pi}_k^{\mathbf{0},K} \boldsymbol{\psi}\|_{\ell,K} \le \zeta \, h_K^{s-\ell} \, |\boldsymbol{\psi}|_{s,K}, \quad 0 \le \ell \le s \le k+1$$
$$\|\psi - \Pi_k^{\nabla,K} \psi\|_{\ell,K} \le \zeta \, h_K^{s-\ell} \, |\psi|_{s,K}, \quad 0 \le \ell \le s \le k+1, \ s \ge 1,$$

*where $\zeta > 0$ only depends on the shape-regularity parameter ρ_0 in assumption (**D1**), and k.*

3.2.4. Global discrete spaces and projectors

The global discrete spaces are defined via their local counterparts:

$$\begin{aligned} \boldsymbol{V}_h &:= \{\boldsymbol{v} \in \boldsymbol{V} : \boldsymbol{v}_{|K} \in \boldsymbol{V}_h(K) \,\forall K \in \mathcal{T}_h\} \\ Q_h &:= \{q \in Q : q_{|K} \in Q_h(K) \,\forall K \in \mathcal{T}_h\} \\ Z_h &:= \{z \in Z : z_{|K} \in Z_h(K) \,\forall K \in \mathcal{T}_h\} \end{aligned}$$

with the obvious sets of global degrees of freedom.

In addition to the broken Sobolev norm (17), we introduce, for all $\boldsymbol{u}_h \in \boldsymbol{V}_h$,

$$\|\boldsymbol{u}_h\|^2_{\boldsymbol{V}_h} := \sum_{K\in\mathcal{T}_h} \|\boldsymbol{u}_h\|^2_{V,K} := \sum_{K\in\mathcal{T}_h} \left[\|\boldsymbol{u}_h\|^2_{0,K} + \|\operatorname{div}\boldsymbol{u}_h\|^2_{0,K}\right].$$

Moreover, we will denote by $\boldsymbol{\Pi}^{\boldsymbol{0}}_{\boldsymbol{k}}$, Π^{∇}_{k+1} and Π^{0}_{k+1}, the global projectors which are defined elementwise as the corresponding local ones in Sections 3.2.2 and 3.2.3.

The sets of global degrees of freedom $\{\mathrm{dof}_j^{\boldsymbol{V}_h}\}_{j=1}^{\dim \boldsymbol{V}_h}$, $\{\mathrm{dof}_j^{Q_h}\}_{j=1}^{\dim Q_h}$, and $\{\mathrm{dof}_j^{Z_h}\}_{j=1}^{\dim Z_h}$ are obtained by coupling the local counterparts given in (20), (21), and (22), respectively.

3.3. Semidiscrete formulation

Our aim in this section is to find a semidiscrete formulation for (10) which is continuous in time and discrete in space. To this purpose, we employ the same notation for the numerical approximants $\boldsymbol{u}_h$, p_h, and c_h, as in (9) for $\boldsymbol{u}$, p, and c, namely

$$\boldsymbol{u}_h(t)(x) := \boldsymbol{u}_h(x,t), \qquad p_h(t)(x) := p_h(x,t), \qquad c_h(t)(x) := c_h(x,t),$$

where the dependence on (t) will be again suppressed in the sequel.

A semidiscrete variational formulation for (10) can then be written in an abstract way as follows: for almost every $t \in J$, find $\boldsymbol{u}_h \in \boldsymbol{V}_h$, $p_h \in Q_h$, and $c_h \in Z_h$, such that

$$\begin{cases} \mathcal{M}_h\left(\dfrac{\partial c_h}{\partial t}, z_h\right) + \Theta_h(\boldsymbol{u}_h, c_h; z_h) + \mathcal{D}_h(\boldsymbol{u}_h; c_h, z_h) = \left(q^+\widehat{c}, z_h\right)_h \\ \mathcal{A}_h(c_h; \boldsymbol{u}_h, \boldsymbol{v}_h) + B(\boldsymbol{v}_h, p_h) = (\boldsymbol{\gamma}(c_h), \boldsymbol{v}_h)_h \\ B(\boldsymbol{u}_h, q_h) = -(G, q_h)_{0,\Omega} \end{cases} \tag{24}$$

for all $\boldsymbol{v}_h \in \boldsymbol{V}_h$, $q_h \in Q_h$, and $z_h \in Z_h$, and the initial condition

$$c_h(0) = c_{0,h} := I_h c_0$$

is satisfied, where $I_h c_0$ is the VEM interpolant of c_0 in Z_h, and where the involved forms and terms in (24) are specified in the forthcoming lines.

Starting from the continuous problem (10), by simply replacing the continuous functions by their discrete counterparts, most of the resulting terms cannot be computed any more, owing to the fact that VE functions are not known explicitly in closed form. Thus, these terms need to be substituted by computable versions in the spirit of the VEM philosophy. To this purpose, the following replacements were made:

- The term $\mathcal{M}\left(\frac{\partial c_h}{\partial t}, z_h\right)$ in the concentration equation was replaced by

$$\mathcal{M}_h\left(\frac{\partial c_h}{\partial t}, z_h\right) := \sum_{K\in\mathcal{T}_h} \mathcal{M}_h^K\left(\frac{\partial c_h}{\partial t}, z_h\right), \tag{25}$$

where the local contributions are given as

$$\begin{aligned} \mathcal{M}_h^K(c_h, z_h) := &\int_K \phi\,(\Pi^{0,K}_{k+1} c_h)\,(\Pi^{0,K}_{k+1} z_h)\,\mathrm{d}x \\ &+ \nu^K_{\mathcal{M}}(\phi) S^K_{\mathcal{M}}\left((I - \Pi^{0,K}_{k+1})c_h, (I - \Pi^{0,K}_{k+1})z_h\right), \end{aligned} \tag{26}$$

with $S^K_{\mathcal{M}}(\cdot,\cdot)$ denoting a stabilization term with certain properties and a constant $\nu^K_{\mathcal{M}}(\phi)$, both described in Section 3.3.1.

- Next, the term $\Theta(\boldsymbol{u}_h, c_h; z_h)$ was substituted by

$$\Theta_h(\boldsymbol{u}_h, c_h; z_h) \coloneqq \frac{1}{2}\Big[(\boldsymbol{u}_h \cdot \nabla c_h, z_h)_h + ((q^+ + q^-)\, c_h, z_h)_h - (\boldsymbol{u}_h\, c_h, \nabla z_h)_h\Big], \tag{27}$$

where

$$\begin{aligned}
(\boldsymbol{u}_h \cdot \nabla c_h, z_h)_h &\coloneqq \sum_{K\in\mathcal{T}_h} \int_K \boldsymbol{\Pi}^{\mathbf{0},K}_{\boldsymbol{k}} \boldsymbol{u}_h \cdot \boldsymbol{\Pi}^{\mathbf{0},K}_{\boldsymbol{k}}(\nabla c_h)\, \Pi^{0,K}_{k+1} z_h \,\mathrm{d}x \\
((q^+ + q^-)\, c_h, z_h)_h &\coloneqq \sum_{K\in\mathcal{T}_h} \int_K (q^+ + q^-)\, \Pi^{0,K}_{k+1} c_h\, \Pi^{0,K}_{k+1} z_h \,\mathrm{d}x \\
(\boldsymbol{u}_h\, c_h, \nabla z_h)_h &\coloneqq \sum_{K\in\mathcal{T}_h} \int_K \boldsymbol{\Pi}^{\mathbf{0},K}_{\boldsymbol{k}} \boldsymbol{u}_h\, \Pi^{0,K}_{k+1} c_h \,\cdot \boldsymbol{\Pi}^{\mathbf{0},K}_{\boldsymbol{k}}(\nabla z_h)\,\mathrm{d}x.
\end{aligned}$$

The above (consistent) choice for Θ_h ensures the coercivity of the bilinear form also at the discrete level.

- Moreover, the term $\mathcal{D}(\boldsymbol{u}_h; c_h, z_h)$ was replaced by

$$\mathcal{D}_h(\boldsymbol{u}_h; c_h, z_h) \coloneqq \sum_{K\in\mathcal{T}_h} \mathcal{D}^K_h(\boldsymbol{u}_h; c_h, z_h) \tag{28}$$

with local contributions

$$\begin{aligned}
\mathcal{D}^K_h(\boldsymbol{u}_h; c_h, z_h) \coloneqq &\int_K D(\boldsymbol{\Pi}^{\mathbf{0},K}_{\boldsymbol{k}}\boldsymbol{u}_h)\, \boldsymbol{\Pi}^{\mathbf{0},K}_{\boldsymbol{k}}(\nabla c_h)\cdot \boldsymbol{\Pi}^{\mathbf{0},K}_{\boldsymbol{k}}(\nabla z_h)\,\mathrm{d}x \\
&+ \nu^K_D(\boldsymbol{u}_h)\, S^K_D\left((I - \Pi^{\nabla,K}_{k+1})c_h, (I - \Pi^{\nabla,K}_{k+1})z_h\right),
\end{aligned} \tag{29}$$

where $S^K_D(\cdot,\cdot)$ is a stabilization term with certain properties and a constant $\nu^K_D(\boldsymbol{u}_h)$, both described in Section 3.3.1.

- Concerning $\left(q^+\widehat{c}, z_h\right)_{0,\Omega}$, this term was approximated by

$$\left(q^+\widehat{c}, z_h\right)_h \coloneqq \sum_{K\in\mathcal{T}_h}\left[\int_K q^+\widehat{c}\,\Pi^{0,K}_{k+1} z_h \,\mathrm{d}x\right].$$

- Regarding the mixed problem, the term $\mathcal{A}(c_h; \boldsymbol{u}_h, \boldsymbol{v}_h)$ was substituted by

$$\mathcal{A}_h(c_h; \boldsymbol{u}_h, \boldsymbol{v}_h) \coloneqq \sum_{K\in\mathcal{T}_h} \mathcal{A}^K_h(c_h; \boldsymbol{u}_h, \boldsymbol{v}_h) \tag{30}$$

with local forms

$$\begin{aligned}
\mathcal{A}^K_h(c_h; \boldsymbol{u}_h, \boldsymbol{v}_h) \coloneqq &\int_K A(\Pi^{0,K}_{k+1} c_h)\boldsymbol{\Pi}^{\mathbf{0},K}_{\boldsymbol{k}}\boldsymbol{u}_h \cdot \boldsymbol{\Pi}^{\mathbf{0},K}_{\boldsymbol{k}}\boldsymbol{v}_h \,\mathrm{d}x \\
&+ \nu^K_{\mathcal{A}}(c_h)\, S^K_{\mathcal{A}}((I - \boldsymbol{\Pi}^{\mathbf{0},K}_{\boldsymbol{k}})\boldsymbol{u}_h, (I - \boldsymbol{\Pi}^{\mathbf{0},K}_{\boldsymbol{k}})\boldsymbol{v}_h),
\end{aligned} \tag{31}$$

where, similarly as before, $S^K_{\mathcal{A}}(\cdot,\cdot)$ is a stabilization term and $\nu^K_{\mathcal{A}}(c_h)$ a constant, both described in Section 3.3.1.

- Finally, the term $(\boldsymbol{\gamma}(c_h), \boldsymbol{v}_h)_{0,\Omega}$ was replaced by

$$(\boldsymbol{\gamma}(c_h), \boldsymbol{v}_h)_h \coloneqq \sum_{K\in\mathcal{T}_h}\left[\int_K \boldsymbol{\gamma}(\Pi^{0,K}_{k+1} c_h)\cdot \boldsymbol{\Pi}^{\mathbf{0},K}_{\boldsymbol{k}}\boldsymbol{v}_h \,\mathrm{d}x\right].$$

At this point, we highlight that the bilinear form $B(\cdot,\cdot)$ needs not to be substituted since it is computable for VE functions due to the choice of degrees of freedom (20). Furthermore, the right hand side term $(G, q_h)_{0,\Omega}$ remains unchanged.

Remark 3.4. Note that we here use the convention that terms which are written in caligraphic letters, such as $\mathcal{M}_h$, $\mathcal{D}_h$ and $\mathcal{A}_h$, include a stabilization term, whereas those in non-caligraphic fashion and those of the form $(\cdot,\cdot)_h$ with subscript h do not. In general, the terms of the type $(\cdot,\cdot)_h$ are approximations of the corresponding (possibly weighted) L^2 scalar products $(\cdot,\cdot)_{0,\Omega}$, obtained by introducing projections onto polynomials for all virtual functions, but not for the data terms that are known exactly.

3.3.1. Construction of the stabilizations

Here, we specify the assumptions on the stabilizations $S^K_{\mathcal{M}}(\cdot,\cdot) : Z_h \times Z_h \to \mathbb{R}$, $S^K_D(\cdot,\cdot) : Z_h \times Z_h \to \mathbb{R}$, and $S^K_{\mathcal{A}}(\cdot,\cdot) : \boldsymbol{V}_h \times \boldsymbol{V}_h \to \mathbb{R}$, in (25), (28), and (30), respectively.

We require that these terms represent computable, symmetric, and positive definite bilinear forms that satisfy, for all $K \in \mathcal{T}_h$, the following property: there exist positive constants $M_0^{\mathcal{M}}$, $M_1^{\mathcal{M}}$, $M_0^{\mathcal{D}}$, $M_1^{\mathcal{D}}$, $M_0^{\mathcal{A}}$, $M_1^{\mathcal{A}}$, which are independent of h and K, such that

$$\begin{aligned} M_0^{\mathcal{M}}\|z_h\|^2_{0,K} \le S^K_{\mathcal{M}}(z_h,z_h) \le M_1^{\mathcal{M}}\|z_h\|^2_{0,K} \qquad & \forall z_h \in Z_h \cap \ker(\Pi^{0,K}_{k+1}) \\ M_0^{\mathcal{D}}\|\nabla z_h\|^2_{0,K} \le S^K_D(z_h,z_h) \le M_1^{\mathcal{D}}\|\nabla z_h\|^2_{0,K} \qquad & \forall z_h \in Z_h \cap \ker(\Pi^{\nabla,K}_{k+1}) \\ M_0^{\mathcal{A}}\|\boldsymbol{v}_h\|^2_{0,K} \le S^K_{\mathcal{A}}(\boldsymbol{v}_h,\boldsymbol{v}_h) \le M_1^{\mathcal{A}}\|\boldsymbol{v}_h\|^2_{0,K} \qquad & \forall \boldsymbol{v}_h \in \boldsymbol{V}_h \cap \ker(\boldsymbol{\Pi}^{\mathbf{0},K}_{k}). \end{aligned} \tag{32}$$

Note that continuity follows immediately from the properties:

$$S^K_{\mathcal{M}}(z_h,\widetilde{z_h}) \le \left(S^K_{\mathcal{M}}(z_h,z_h)\right)^{\frac{1}{2}} \left(S^K_{\mathcal{M}}(\widetilde{z_h},\widetilde{z_h})\right)^{\frac{1}{2}} \le M_1^{\mathcal{M}}\|z_h\|_{0,K}\|\widetilde{z_h}\|_{0,K}$$

for all $z_h, \widetilde{z_h} \in Z_h \cap \ker(\Pi^{0,K}_{k+1})$; analogously for the other forms. In practice, under mesh assumptions (**D1**)–(**D2**), one can take the following scaled stabilizations corresponding to the degrees of freedom:

$$\begin{aligned} S^K_{\mathcal{M}}(c_h,z_h) &= |K| \sum_{j=1}^{\dim Z_h(K)} \mathrm{dof}_j^{Z_h(K)}(c_h)\,\mathrm{dof}_j^{Z_h(K)}(z_h) \\ S^K_D(c_h,z_h) &= \sum_{j=1}^{\dim Z_h(K)} \mathrm{dof}_j^{Z_h(K)}(c_h)\,\mathrm{dof}_j^{Z_h(K)}(z_h) \\ S^K_{\mathcal{A}}(\boldsymbol{u}_h,\boldsymbol{v}_h) &= |K| \sum_{j=1}^{\dim \boldsymbol{V}_h(K)} \mathrm{dof}_j^{\boldsymbol{V}_h(K)}(\boldsymbol{u}_h)\,\mathrm{dof}_j^{\boldsymbol{V}_h(K)}(\boldsymbol{v}_h). \end{aligned} \tag{33}$$

Regarding the constants appearing in front of the stabilizations in (25), (28), and (30), respectively, we pick:

$$\nu^K_{\mathcal{M}}(\phi) = \left|\Pi^{0,K}_0\phi\right|, \quad \nu^K_D(\boldsymbol{u}_h) = \nu^K_{\mathcal{M}}(\phi)(d_m + d_t|\boldsymbol{\Pi}^{\mathbf{0},K}_{\mathbf{0}}\boldsymbol{u}_h|), \quad \nu^K_{\mathcal{A}}(c_h) = |A(\Pi^{0,K}_0(c_h))|, \tag{34}$$

where $\Pi^{0,K}_0 : L^2(K) \to \mathbb{P}_0(K)$ and $\boldsymbol{\Pi}^{\mathbf{0},K}_{\mathbf{0}} : [L^2(K)]^2 \to [\mathbb{P}_0(K)]^2$ are the L^2 projectors onto scalar and vector valued constants, respectively. The values appearing in (34) are positive constants that are introduced in order to take into account the material amplitudes in the stabilizations. Since the amplitudes of some material coefficients depend on the solution (the problem is nonlinear), such values are taken in accordance, and turn out to depend on the discrete solution.

3.3.2. Well-posedness of the semidiscrete problem

We firstly define the constants

$$\nu^-_{\mathcal{M}} := \min_{K\in\mathcal{T}_h} \nu^K_{\mathcal{M}}, \qquad \nu^+_{\mathcal{M}} := \max_{K\in\mathcal{T}_h} \nu^K_{\mathcal{M}}.$$

Analogously, we introduce $\nu^-_{\mathcal{D}}$, $\nu^+_{\mathcal{D}}$, $\nu^-_{\mathcal{A}}$m and $\nu^+_{\mathcal{A}}$. Recalling (3) and (6), it is easy to check the following (mesh-uniform) bounds for the above constants:

$$\begin{aligned} &\phi_* \le \nu^-_{\mathcal{M}} \le \nu^+_{\mathcal{M}} \le \phi^*, \quad (a^*)^{-1} \le \nu^-_{\mathcal{A}} \le \nu^+_{\mathcal{A}} \le a_*^{-1} \\ &\phi_* d_m \le \nu^-_{\mathcal{D}} \le \nu^+_{\mathcal{D}} \le \phi^*(d_m + (d_\ell + d_t)\|\boldsymbol{u}_h\|_{\infty,\Omega}). \end{aligned}$$

Then, similarly as for their continuous counterparts, the following continuity and coercivity properties for $\mathcal{M}_h(\cdot,\cdot)$ $\mathcal{D}_h(\cdot;\cdot,\cdot)$, and $\mathcal{A}_h(\cdot;\cdot,\cdot)$, defined in (25), (28), and (30), respectively, hold true.

Lemma 3.2. *For $\mathcal{M}_h(\cdot,\cdot)$, it holds, for all $c_h, z_h \in Z_h$,*

$$\begin{aligned} &\mathcal{M}_h(c_h,z_h) \le \max\{\phi^*, \nu^+_{\mathcal{M}}M_1^{\mathcal{M}}\}\|c_h\|_{0,\Omega}\|z_h\|_{0,\Omega} \\ &\mathcal{M}_h(z_h,z_h) \ge \min\{\phi_*, \nu^-_{\mathcal{M}}M_0^{\mathcal{M}}\}\|z_h\|^2_{0,\Omega}. \end{aligned} \tag{35}$$

Concerning $\mathcal{D}_h(\cdot;\cdot,\cdot)$, this form satisfies, for all $\boldsymbol{u}_h \in \boldsymbol{V}_h$ and $c_h, z_h \in Z_h$,

$$\begin{aligned}\mathcal{D}_h(\boldsymbol{u}_h; c_h, z_h) &\leq \left[\phi^*\left(d_m + \eta\|\boldsymbol{u}_h\|_{\infty,\Omega}(d_\ell + d_t)\right) + \nu_{\mathcal{D}}^+ M_1^{\mathcal{D}}\right]|c_h|_{1,\mathcal{T}_h}|z_h|_{1,\mathcal{T}_h}\\ \mathcal{D}_h(\boldsymbol{u}_h; z_h, z_h) &\geq \min\{\phi_* d_m, \nu_{\mathcal{D}}^- M_0^{\mathcal{D}}\}|z_h|_{1,\mathcal{T}_h}^2.\end{aligned} \tag{36}$$

Regarding $\mathcal{A}_h(\cdot;\cdot,\cdot)$, for all $c_h \in Z_h$ and $\boldsymbol{u}_h, \boldsymbol{v}_h \in \boldsymbol{V}_h$, it yields

$$\begin{aligned}\mathcal{A}_h(c_h; \boldsymbol{u}_h, \boldsymbol{v}_h) &\leq \max\left\{\frac{1}{a_*}, \nu_{\mathcal{A}}^+ M_1^{\mathcal{A}}\right\}\|\boldsymbol{u}_h\|_{0,\Omega}\|\boldsymbol{v}_h\|_{0,\Omega}\\ \mathcal{A}_h(c_h; \boldsymbol{v}_h, \boldsymbol{v}_h) &\geq \min\left\{\frac{1}{a^*}, \nu_{\mathcal{A}}^- M_0^{\mathcal{A}}\right\}\|\boldsymbol{v}_h\|_{0,\Omega}^2.\end{aligned} \tag{37}$$

Thus, $\mathcal{A}_h(c_h;\cdot,\cdot)$ is coercive on the kernel

$$\mathcal{K}_h := \{\boldsymbol{v}_h \in \boldsymbol{V}_h : B(\boldsymbol{v}_h, q_h) = 0 \quad \forall q_h \in Q_h\} \subset \mathcal{K} \tag{38}$$

with respect to $\|\cdot\|_{\boldsymbol{V}_h}$, where $\mathcal{K}$ is given in (13).

Proof. The continuity bound in (35) follows directly by using

$$\mathcal{M}_h(c_h, z_h) \leq \mathcal{M}_h(c_h, c_h)^{\frac{1}{2}}\mathcal{M}_h(z_h, z_h)^{\frac{1}{2}}, \tag{39}$$

and then estimating

$$\begin{aligned}\mathcal{M}_h(c_h, c_h) &\leq \phi^*\|\Pi_{k+1}^{0,K} c_h\|_{0,K}^2 + \nu_{\mathcal{M}}^+ M_1^{\mathcal{M}}\|(I - \Pi_{k+1}^{0,K})c_h\|_{0,K}^2\\ &\leq \max\{\phi^*, \nu_{\mathcal{M}}^+ M_1^{\mathcal{M}}\}\left(\|\Pi_{k+1}^{0,K} c_h\|_{0,K}^2 + \|(I - \Pi_{k+1}^{0,K})c_h\|_{0,K}^2\right)\\ &= \max\{\phi^*, \nu_{\mathcal{M}}^+ M_1^{\mathcal{M}}\}\|c_h\|_{0,K}^2,\end{aligned}$$

where the Pythagorean theorem was applied in the last equality. For the coercivity bound, one can use (6), (32), and the Pythagorean theorem.

Regarding the continuity estimate for $\mathcal{D}_h(\cdot;\cdot,\cdot)$, by using a splitting of the form (39), together with an estimate as in (14), one can deduce at the local level

$$\begin{aligned}\mathcal{D}_h^K(\boldsymbol{u}_h; c_h, c_h) &\leq \phi^*\left(d_m + \eta\|\boldsymbol{\Pi}_{\boldsymbol{k}}^{\boldsymbol{0},\boldsymbol{K}}\boldsymbol{u}_h\|_{\infty,\Omega}(d_\ell + d_t)\right)\|\boldsymbol{\Pi}_{\boldsymbol{k}}^{\boldsymbol{0},\boldsymbol{K}}(\nabla c_h)\|_{0,K}^2\\ &\quad + \left(\nu_{\mathcal{D}}^+ M_1^{\mathcal{D}}\right)\|\nabla(I - \Pi_{k+1}^{\nabla,K})c_h\|_{0,K}^2\\ &\leq \left[\phi^*\left(d_m + \eta\|\boldsymbol{\Pi}_{\boldsymbol{k}}^{\boldsymbol{0},\boldsymbol{K}}\boldsymbol{u}_h\|_{\infty,\Omega}(d_\ell + d_t)\right) + \nu_{\mathcal{D}}^+ M_1^{\mathcal{D}}\right]|c_h|_{1,\mathcal{T}_h}^2.\end{aligned} \tag{40}$$

By application of a polynomial inverse estimate [65, Lemma 4.5.3], the continuity of the L^2 projector, and the Hölder inequality, we further estimate

$$\|\boldsymbol{\Pi}_{\boldsymbol{k}}^{\boldsymbol{0},\boldsymbol{K}}\boldsymbol{u}_h\|_{\infty,K} \leq \eta\, h_K^{-1}\|\boldsymbol{\Pi}_{\boldsymbol{k}}^{\boldsymbol{0},\boldsymbol{K}}\boldsymbol{u}_h\|_{0,K} \leq \eta\, h_K^{-1}\|\boldsymbol{u}_h\|_{0,K} \leq \eta\|\boldsymbol{u}_h\|_{\infty,K}. \tag{41}$$

After inserting (41) into (40), taking the splitting into account, and summing over all elements, the stated bound follows. Concerning the coercivity bound for $\mathcal{D}_h(\cdot,\cdot)$, one can proceed similarly as in (16) for the consistency part, and employ (32) for the stabilization term, to obtain elementwise

$$\mathcal{D}_h^K(\boldsymbol{u}_h; z_h, z_h) \geq \min\{\phi_* d_m, \nu_{\mathcal{D}}^- M_0^{\mathcal{D}}\}\left[\|\boldsymbol{\Pi}_{\boldsymbol{k}}^{\boldsymbol{0},\boldsymbol{K}}\nabla z_h\|_{0,K}^2 + \|\nabla(I - \Pi_{k+1}^{\nabla,K})z_h\|_{0,K}^2\right].$$

We now note that the definitions of $\Pi_{k+1}^{\nabla,K}$ and $\boldsymbol{\Pi}_{\boldsymbol{k}}^{\boldsymbol{0},\boldsymbol{K}}$ easily yield

$$\|\nabla(I - \Pi_{k+1}^{\nabla,K})z_h\|_{0,K} \geq \|(I - \boldsymbol{\Pi}_{\boldsymbol{k}}^{\boldsymbol{0},\boldsymbol{K}})\nabla z_h\|_{0,K}. \tag{42}$$

The estimate then follows with (42), the Pythagorean theorem and summation over all elements.

The estimates for $\mathcal{A}_h(\cdot;\cdot,\cdot)$ are derived in a similar fashion as those for $\mathcal{M}_h(\cdot,\cdot)$, using (6). The coercivity on $\mathcal{K}_h$ follows from the fact

$$\mathcal{K}_h \equiv \{\boldsymbol{v}_h \in \boldsymbol{V}_h : \operatorname{div}\boldsymbol{v}_h = 0\} \subset \mathcal{K},$$

owing to the definition of $\boldsymbol{V}_h(K)$ in (18). □

Well-posedness of problem (24) can be shown by combining the results in [20] for parabolic problems with those in [17,50] for mixed problems, using Lemma 3.2. More precisely, in the spirit of the two-step strategy applied in [31] for FEM, one can first show that for any given $c_h(t) \in L^\infty(\Omega)$, $t \in J$, the mixed problem

$$\begin{aligned} \mathcal{A}_h(c_h; \boldsymbol{u}_h, \boldsymbol{v}_h) + B(\boldsymbol{v}_h, p_h) &= (\boldsymbol{\gamma}(c_h), \boldsymbol{v}_h)_h \\ B(\boldsymbol{u}_h, q_h) &= -(G, q_h)_{0,\Omega} \end{aligned}$$

admits a unique solution by applying the techniques in [17,50], and then, by using the Gronwall lemma and Picard–Lindelöf (see e.g. [66, Ch.1.10]), that $c_h(t)$ is uniquely determined by the discrete concentration equation

$$\mathcal{M}_h\left(\frac{\partial c_h}{\partial t}, z_h\right) + \Theta_h(\boldsymbol{u}_h, c_h; z_h) + \mathcal{D}_h(\boldsymbol{u}_h; c_h, z_h) = \left(q^+ \widehat{c}, z_h\right)_h,$$

see also [20]. We do not write here the details since we focus directly on the fully discrete case, see the next section.

3.4. Fully discrete formulation

Here, our goal is to formulate a fully discrete version of (24). To start with, we introduce a sequence of time steps $t_n = n\tau$, $n = 0, \dots, N$, with time step size τ. Next, we define $\boldsymbol{u}^n := \boldsymbol{u}(t_n)$, $p^n := p(t_n)$, $c^n := c(t_n)$, $G^n := G(t_n)$, $(q^+)^n := q^+(t_n)$, and $\widehat{c}^n := \widehat{c}(t_n)$ as the evaluations of the corresponding functions at time t_n, $n = 0, \dots, N$. Moreover, we denote by $\boldsymbol{U}^n \approx \boldsymbol{u}_h(t_n)$, $P^n \approx p_h(t_n)$, and $C^n \approx c_h(t_n)$, the approximations of the semidiscrete solutions at those times when using a time integrator method $\mathcal{I}$. The error generated by a fully discrete scheme has two components: the error due to the VEM spatial discretization depending on the mesh size h, and the error produced by the numerical scheme $\mathcal{I}$ depending on the time step size τ. Then we expect that for sufficiently regular solution (u, p, c) one has

$$\|\boldsymbol{u}^n - \boldsymbol{U}^n\|_{0,\Omega} + \|p^n - P^n\|_{0,\Omega} + \|c^n - C^n\|_{1,\Omega} \le C_1 h^{k+1} + C_2 \tau^s \tag{43}$$

where s is the order of the method $\mathcal{I}$, and C_1 and C_2 are two h and τ independent constants. Since the novelty of the present paper is the VEM discretization, we focus mainly on the spatial source of error. Among many time discretization schemes, in order to detail the behavior of the method, we here make a computationally cheap choice by choosing a backward Euler method that is explicit in the nonlinear terms. As a consequence, we obtain two "smaller" linear systems at each time step, instead of a single larger nonlinear system (as one would obtain with a fully coupled implicit backward Euler scheme). However, accordingly with (43), more advanced higher order time integrator scheme can be adopted as well.

The fully discrete system consequently reads as follows:

- for $n = 0$: Given $c_{0,h} \in Z_h$, solve

$$\begin{aligned} \mathcal{A}_h(c_{0,h}; \boldsymbol{U}^n, \boldsymbol{v}_h) + B(\boldsymbol{v}_h, P^n) &= (\boldsymbol{\gamma}(c_{0,h}), \boldsymbol{v}_h)_h \\ B(\boldsymbol{U}^n, q_h) &= -\left(G^n, q_h\right)_{0,\Omega} \end{aligned} \tag{44}$$

  for all $\boldsymbol{v}_h \in \boldsymbol{V}_h$ and $q_h \in Q_h$.
- for $n = 1, \dots, N$: Solve first the concentration equation for C^n:

$$\mathcal{M}_h\left(\frac{C^n - C^{n-1}}{\tau}, z_h\right) + \Theta_h(\boldsymbol{U}^{n-1}; C^n, z_h) + \mathcal{D}_h(\boldsymbol{U}^{n-1}; C^n, z_h) = \left((q^+)^n \widehat{c}^n, z_h\right)_h, \tag{45}$$

  for all $z_h \in Z_h$, where $C^0 := c_{0,h}$. Then, solve the mixed problem for $\boldsymbol{U}^n$ and P^n:

$$\begin{aligned} \mathcal{A}_h(C^n; \boldsymbol{U}^n, \boldsymbol{v}_h) + B(\boldsymbol{v}_h, P^n) &= (\boldsymbol{\gamma}(C^n), \boldsymbol{v}_h)_h \\ B(\boldsymbol{U}^n, q_h) &= -\left(G^n, q_h\right)_{0,\Omega}, \end{aligned} \tag{46}$$

  for all $\boldsymbol{v}_h \in \boldsymbol{V}_h$ and $q_h \in Q_h$.

Lemma 3.3. *Given $\tau > 0$, provided that $G^n, (q^+)^n, P^n, C^n \in L^\infty(\Omega)$, $\boldsymbol{\gamma}(C^n) \in [L^2(\Omega)]^2$, and $\boldsymbol{U}^n \in [L^\infty(\Omega)]^2$, for all $n = 0, \dots, N$, the formulation (44)–(46) is uniquely solvable.*

Proof. Similarly as for the semidiscrete case, well-posedness of (44) and (46) follows by using the tools of [17,50]. Regarding (45), we firstly rewrite that equation as

$$\begin{aligned}\mathcal{M}_h\left(C^n, z_h\right) + \tau\left[\Theta_h(\boldsymbol{U}^{n-1}; C^n, z_h) + \mathcal{D}_h(\boldsymbol{U}^{n-1}; C^n, z_h)\right] \\ = \tau\left((q^+)^n \widehat{c}^n, z_h\right)_h + \mathcal{M}_h\left(C^{n-1}, z_h\right).\end{aligned} \tag{47}$$

We observe that all of the terms are continuous with respect to the norm $\|\cdot\|_{1,\mathcal{T}_h}$. More precisely, for $\mathcal{M}_h(\cdot,\cdot)$ and $\mathcal{D}_h(\boldsymbol{U}^{n-1};\cdot,\cdot)$, continuity follows from Lemma 3.2 and the definition of the broken H^1 norm. Next, for the term involving $(q^+)^n$, we simply apply the Cauchy–Schwarz inequality and the stability of the L^2 projector. Finally, for the term with Θ_h, we estimate

$$\begin{aligned}\Theta_h(\boldsymbol{U}^{n-1}; C^n, z_h) &= \frac{1}{2}\left[\left(\boldsymbol{U}^{n-1}\cdot\nabla C^n, z_h\right)_h + ((q^+ + q^-)\, C^n, z_h)_h - \left(\boldsymbol{U}^{n-1} C^n, \nabla z_h\right)_h\right] \\ &\leq \eta\left[\|\boldsymbol{U}^{n-1}\|_{\infty,\Omega}(|C^n|_{1,\mathcal{T}_h} + \|C^n\|_{0,\Omega}) + \|q^+ + q^-\|_{\infty,\Omega}\|C^n\|_{0,\Omega}\right]\|z_h\|_{1,\mathcal{T}_h},\end{aligned}$$

where we also employed an inverse inequality as in (41). Thus, by the Lax–Milgram lemma, it only remains to show that the left hand side of (47) is coercive with respect to $\|\cdot\|_{1,\mathcal{T}_h}$. This is however a direct consequence of

$$\Theta_h(\boldsymbol{U}^{n-1}; z_h, z_h) = \frac{1}{2}((q^+ + q^-)\, z_h, z_h)_h \geq 0,$$

owing to the fact that q^+ and q^- are non-negative, and the coercivity bounds (35) and (36). □

Note that both problems (45) and (46) represent linear systems of equations which are decoupled from each other in the sense that, firstly, given $\widehat{c}^n$ and $(q^+)^n$, one can determine C^n with knowledge of $\boldsymbol{U}^{n-1}$ only, and then one can use C^n to compute $\boldsymbol{U}^n$ and P^n. The quantity P^n does in fact not influence the calculation of C^n directly, but rather takes the role of a Lagrange multiplier and derived variable. This decoupling, combined with the fact that the systems to be solved at each time step are linear, makes the method quite cheap per iteration.

4. Error analysis for the fully discrete problem

The error analysis is performed in two steps: firstly, we estimate the discretization errors for the velocity and pressure, $\|\boldsymbol{u}^n - \boldsymbol{U}^n\|_{0,\Omega}$ and $\|p^n - P^n\|_{0,\Omega}$, respectively, and then, in the second step, the concentration error $\|c^n - C^n\|_{0,\Omega}$. In the following analysis, we assume all the needed regularity of the exact solution. Although such high regularity will not often be available in practice, the purpose of the following analysis is to give a theoretical backbone to the proposed scheme and to investigate its potential accuracy in the most favorable scenario.

4.1. An auxiliary result

The subsequent technical lemma will serve as an auxiliary result in the derivation of the error estimates and will be used in several occasions.

Lemma 4.1. *Let $r, s, t \in \mathbb{N}_0$. Denote by Π_r^0 and $\boldsymbol{\Pi}_s^{\mathbf{0}}$, the elementwise defined L^2 projectors onto scalar and vector valued polynomials of degree at most r and s, respectively. Given a scalar function $\sigma \in H^{m_r}(\mathcal{T}_h)$, $0 \leq m_r \leq r+1$, let $\kappa(\sigma)$ be a tensor valued piecewise Lipschitz continuous function with respect to σ. Further, let $\widehat{\sigma} \in L^2(\Omega)$, and let $\boldsymbol{\chi}$ and $\boldsymbol{\psi}$ be vector valued functions. We assume that $\kappa(\sigma) \in [L^\infty(\Omega)]^{2\times 2}$, $\boldsymbol{\chi} \in [H^{m_s}(\mathcal{T}_h) \cap L^\infty(\Omega)]^2$, $\boldsymbol{\psi} \in [L^2(\Omega)]^2$, and $\kappa(\sigma)\boldsymbol{\chi} \in [H^{m_t}(\mathcal{T}_h)]^2$, for some $0 \leq m_s \leq s+1$ and $0 \leq m_t \leq t+1$. Then,*

$$\begin{aligned}&(\kappa(\sigma)\boldsymbol{\chi}, \boldsymbol{\psi})_{0,\Omega} - (\kappa(\Pi_r^0\widehat{\sigma})\boldsymbol{\Pi}_s^{\mathbf{0}}\boldsymbol{\chi}, \boldsymbol{\Pi}_t^{\mathbf{0}}\boldsymbol{\psi})_{0,\Omega} \\ &\leq \eta\left[h^{m_t}|\kappa(\sigma)\boldsymbol{\chi}|_{m_t,\mathcal{T}_h} + h^{m_s}|\boldsymbol{\chi}|_{m_s,\mathcal{T}_h}\|\kappa(\sigma)\|_{\infty,\Omega} + (h^{m_r}|\sigma|_{m_r,\mathcal{T}_h} + \|\sigma - \widehat{\sigma}\|_{0,\Omega})\|\boldsymbol{\chi}\|_{\infty,\Omega}\right]\|\boldsymbol{\psi}\|_{0,\Omega}.\end{aligned}$$

Proof. We firstly write

$$\begin{aligned}&(\kappa(\sigma)\boldsymbol{\chi}, \boldsymbol{\psi})_{0,\Omega} - (\kappa(\Pi_r^0\widehat{\sigma})\boldsymbol{\Pi}_s^{\mathbf{0}}\boldsymbol{\chi}, \boldsymbol{\Pi}_t^{\mathbf{0}}\boldsymbol{\psi})_{0,\Omega} \\ &= [(\kappa(\sigma)\boldsymbol{\chi}, \boldsymbol{\psi})_{0,\Omega} - (\kappa(\Pi_r^0\sigma)\boldsymbol{\Pi}_s^{\mathbf{0}}\boldsymbol{\chi}, \boldsymbol{\Pi}_t^{\mathbf{0}}\boldsymbol{\psi})_{0,\Omega}] + ((\kappa(\Pi_r^0\sigma) - \kappa(\Pi_r^0\widehat{\sigma}))\boldsymbol{\Pi}_s^{\mathbf{0}}\boldsymbol{\chi}, \boldsymbol{\Pi}_t^{\mathbf{0}}\boldsymbol{\psi})_{0,\Omega}.\end{aligned} \tag{48}$$

Then, for the first part on the right hand side of (48), we recall that $\mathbf{\Pi}_t^{\mathbf{0}}$ is an L^2 projection and derive, on each element $K \in \mathcal{T}_h$,

$$
\begin{aligned}
&(\kappa(\sigma)\boldsymbol{\chi}, \boldsymbol{\psi})_{0,K} - (\kappa(\Pi_r^{0,K}\sigma)\mathbf{\Pi}_s^{\mathbf{0},\boldsymbol{K}}\boldsymbol{\chi}, \mathbf{\Pi}_t^{\mathbf{0},\boldsymbol{K}}\boldsymbol{\psi})_{0,K} \\
&= [(\kappa(\sigma)\boldsymbol{\chi}, \boldsymbol{\psi})_{0,K} - (\mathbf{\Pi}_t^{\mathbf{0},\boldsymbol{K}}(\kappa(\sigma)\boldsymbol{\chi}), \boldsymbol{\psi})_{0,K}] \\
&\quad + [(\mathbf{\Pi}_t^{\mathbf{0},\boldsymbol{K}}(\kappa(\sigma)\boldsymbol{\chi}), \boldsymbol{\psi})_{0,K} - (\mathbf{\Pi}_t^{\mathbf{0},\boldsymbol{K}}(\kappa(\sigma)\mathbf{\Pi}_s^{\mathbf{0},\boldsymbol{K}}\boldsymbol{\chi}), \boldsymbol{\psi})_{0,K}] \\
&\quad + [(\mathbf{\Pi}_t^{\mathbf{0},\boldsymbol{K}}(\kappa(\sigma)\mathbf{\Pi}_s^{\mathbf{0},\boldsymbol{K}}\boldsymbol{\chi}), \boldsymbol{\psi})_{0,K} - (\mathbf{\Pi}_t^{\mathbf{0},\boldsymbol{K}}(\kappa(\Pi_r^{0,K}\sigma)\mathbf{\Pi}_s^{\mathbf{0},\boldsymbol{K}}\boldsymbol{\chi}), \boldsymbol{\psi})_{0,K}] \\
&\leq \eta\big[h^{m_t}|\kappa(\sigma)\boldsymbol{\chi}|_{m_t,K} + h^{m_s}|\boldsymbol{\chi}|_{m_s,K}\|\kappa(\sigma)\|_{\infty,K} + h^{m_r}|\sigma|_{m_r,K}\|\mathbf{\Pi}_s^{\mathbf{0},\boldsymbol{K}}\boldsymbol{\chi}\|_{\infty,K}\big]\|\boldsymbol{\psi}\|_{0,K},
\end{aligned}
$$

where in the last step we used Lemma 3.1 and the fact that κ is Lipschitz continuous with respect to σ. The term $\|\mathbf{\Pi}_s^{\mathbf{0},\boldsymbol{K}}\boldsymbol{\chi}\|_{\infty,K}$ is estimated as in (41). Concerning the second part on the right hand side of (48), we have, for each $K \in \mathcal{T}_h$,

$$
\begin{aligned}
((\kappa(\Pi_r^0\sigma) - \kappa(\Pi_r^0\widehat{\sigma}))\mathbf{\Pi}_s^{\mathbf{0}}\boldsymbol{\chi}, \mathbf{\Pi}_t^{\mathbf{0}}\boldsymbol{\psi})_{0,K} &\leq \|\kappa(\Pi_r^0\sigma) - \kappa(\Pi_r^0\widehat{\sigma})\|_{0,K}\|\mathbf{\Pi}_s^{\mathbf{0}}\boldsymbol{\chi}\|_{\infty,K}\|\mathbf{\Pi}_t^{\mathbf{0}}\boldsymbol{\psi}\|_{0,K} \\
&\leq \|\sigma - \widehat{\sigma}\|_{0,K}\|\boldsymbol{\chi}\|_{\infty,K}\|\boldsymbol{\psi}\|_{0,K},
\end{aligned}
$$

where we used again the Lipschitz continuity of κ, the continuity properties of the L^2 projectors, and the bound (41). The assertion of the lemma follows after combining the estimates and summing over all elements. □

Note that the above lemma can be easily transferred to the cases where σ, $\kappa(\sigma)$, χ, and ψ are scalar, and to vector valued $\boldsymbol{\sigma}$, $\boldsymbol{\chi}$ and scalar $\kappa(\boldsymbol{\sigma})$, ψ.

In the special case of $\chi = 1$ and vector valued $\boldsymbol{\kappa}$, an adaptation of Lemma 4.1 gives

$$
(\boldsymbol{\kappa}(\sigma), \boldsymbol{\psi})_{0,\Omega} - (\boldsymbol{\kappa}(\Pi_r^0\widehat{\sigma}), \mathbf{\Pi}_t^{\mathbf{0}}\boldsymbol{\psi})_{0,\Omega} \leq \eta\big[h^{m_t}|\boldsymbol{\kappa}(\sigma)|_{m_t,\mathcal{T}_h} + h^{m_r}|\sigma|_{m_r,\mathcal{T}_h} + \|\sigma - \widehat{\sigma}\|_{0,\Omega}\big]\|\boldsymbol{\psi}\|_{0,\Omega}. \tag{49}
$$

4.2. Error bounds: velocity and pressure

We consider the mixed problem

$$
\begin{aligned}
\mathcal{A}_h(C^n; \boldsymbol{U}^n, \boldsymbol{v}_h) + B(\boldsymbol{v}_h, P^n) &= (\boldsymbol{\gamma}(C^n), \boldsymbol{v}_h)_h \\
B(\boldsymbol{U}^n, q_h) &= -\left(G^n, q_h\right)_{0,\Omega},
\end{aligned} \tag{50}
$$

where $C^n \in Z_h$ is the numerical solution of the concentration equation (45) for $n = 1, \ldots, N$, and $C^0 = c_{0,h}$. The goal is to derive an upper bound for $\|\boldsymbol{u}^n - \boldsymbol{U}^n\|_{0,\Omega}$ and $\|p^n - P^n\|_{0,\Omega}$ with respect to $\|c^n - C^n\|_{0,\Omega}$. For the analysis, we basically follow the ideas of [17,50] with the major differences that, here, $\mathcal{A}_h(C^n; \cdot, \cdot)$ is not consistent with respect to $[\mathbb{P}_k(K)]^2$ due to presence of C^n, and, additionally, the right hand side of (50) is inhomogeneous.

Theorem 1. *Given $C^n \in Z_h$, let $(\boldsymbol{U}^n, P^n) \in \boldsymbol{V}_h \times Q_h$ be the solution to (50). Let us assume that for the exact solution $(\boldsymbol{u}^n, p^n, c^n)$ to (10) at time t_n, it holds $\boldsymbol{u}^n \in [H^{k+1}(\mathcal{T}_h)]^2$, $p^n \in H^{k+1}(\mathcal{T}_h)$, and $c^n \in H^{k+1}(\mathcal{T}_h)$. Furthermore, we suppose that $\boldsymbol{\gamma}(c)$ and $A(c)$ are piecewise Lipschitz continuous functions with respect to $c \in L^2(\Omega)$, and that $\boldsymbol{\gamma}(c^n)$, $A(c^n)\boldsymbol{u}^n \in [H^{k+1}(\mathcal{T}_h)]^2$. Then, the following error estimates hold for all $k \in \mathbb{N}_0$:*

$$
\begin{aligned}
\|\boldsymbol{U}^n - \boldsymbol{u}^n\|_{0,\Omega} &\leq \|C^n - c^n\|_{0,\Omega}\,\zeta_1^n(\boldsymbol{u}^n) + h^{k+1}\,\zeta_2^n(\boldsymbol{u}^n, c^n, \boldsymbol{\gamma}(c^n), A(c^n)\boldsymbol{u}^n) \\
\|P^n - p^n\|_{0,\Omega} &\leq \|C^n - c^n\|_{0,\Omega}\,\zeta_3^n(\boldsymbol{u}^n) + h^{k+1}\,\zeta_4^n(\boldsymbol{u}^n, c^n, \boldsymbol{\gamma}(c^n), A(c^n)\boldsymbol{u}^n, p^n),
\end{aligned}
$$

where ζ_1^n–ζ_4^n are positive constants independent of h and depending only on the specified functions.

Proof. The estimate for $\|\boldsymbol{U}^n - \boldsymbol{u}^n\|_{0,\Omega}$ can be obtained as follows:

By using the second equality in (50), we have $\operatorname{div}\boldsymbol{U}^n = \Pi_k^0 G^n$ (use that $\operatorname{div}\boldsymbol{U}^n \in \mathbb{P}_k(K)$ for every $K \in \mathcal{T}_h$), where we recall that $(\Pi_k^0)_{|K} = \Pi_k^{0,K}$. Define now the interpolant $\boldsymbol{u}_I^n \in \boldsymbol{V}_h$ via the degrees of freedom (20):

$$
\operatorname{dof}_i^{\boldsymbol{V}_h}(\boldsymbol{u}_I^n) = \operatorname{dof}_i^{\boldsymbol{V}_h}(\boldsymbol{u}^n), \quad i = 1, \ldots, \dim\boldsymbol{V}_h.
$$

Then, it holds [17, Eq. (28)]

$$
\|\boldsymbol{u}^n - \boldsymbol{u}_I^n\|_{0,\Omega} \leq \eta\, h^{k+1}\|\boldsymbol{u}^n\|_{k+1,\mathcal{T}_h}. \tag{51}
$$

Moreover, one has $\operatorname{div} \boldsymbol{u}_I^n = \Pi_k^0 G^n$. Thus, setting $\boldsymbol{\delta}^n := \boldsymbol{U}^n - \boldsymbol{u}_I^n$, it holds that $\boldsymbol{\delta}^n \in \mathcal{K}_h \subset \mathcal{K}$, where $\mathcal{K}_h$ and $\mathcal{K}$ were defined in (38) and (13), respectively, therefore $B(\boldsymbol{\delta}^n, q) = 0$ for all $q \in Q$ and $\|\boldsymbol{\delta}^n\|_{V_h} = \|\boldsymbol{\delta}^n\|_{0,\Omega}$. Owing to the assumptions on $a(\cdot)$ in (6) together with (37), we have, further using (50) with $\boldsymbol{v}_h = \boldsymbol{\delta}^n \in \mathcal{K}_h$ and (10),

$$\begin{aligned}
\alpha \|\boldsymbol{\delta}^n\|_{0,\Omega}^2 &\le \mathcal{A}_h(C^n; \boldsymbol{\delta}^n, \boldsymbol{\delta}^n) = \mathcal{A}_h(C^n; \boldsymbol{U}^n, \boldsymbol{\delta}^n) - \mathcal{A}_h(C^n; \boldsymbol{u}_I^n, \boldsymbol{\delta}^n) \\
&= (\boldsymbol{\gamma}(C^n), \boldsymbol{\delta}^n)_h - \mathcal{A}_h(C^n; \boldsymbol{u}_I^n, \boldsymbol{\delta}^n) \\
&= \big[(\boldsymbol{\gamma}(C^n), \boldsymbol{\delta}^n)_h - (\boldsymbol{\gamma}(c^n), \boldsymbol{\delta}^n)_{0,\Omega}\big] + \mathcal{A}_h(C^n; \boldsymbol{u}^n - \boldsymbol{u}_I^n, \boldsymbol{\delta}^n) \\
&\quad + \Big[\mathcal{A}(c^n; \boldsymbol{u}^n, \boldsymbol{\delta}^n) - \mathcal{A}_h(C^n; \boldsymbol{u}^n, \boldsymbol{\delta}^n)\Big] \\
&=: T_1 + T_2 + T_3.
\end{aligned} \tag{52}$$

The terms T_1–T_3 are bounded as follows:

- term T_1: We use Eq. (49) with $\boldsymbol{\kappa} = \boldsymbol{\gamma}$, $\sigma = c^n$, $\widehat{\sigma} = C^n$, $\boldsymbol{\psi} = \boldsymbol{\delta}^n$, $r = k+1$, $t = k$, and $m_r = m_t = k+1$, and obtain

$$\begin{aligned}
|T_1| &= |(\boldsymbol{\gamma}(c^n), \boldsymbol{\delta}^n)_{0,\Omega} - (\boldsymbol{\gamma}(\Pi_{k+1}^0 C^n), \boldsymbol{\Pi}_k^{\mathbf{0}} \boldsymbol{\delta}^n)_{0,\Omega}| \\
&\le \eta \big[h^{k+1}(|\boldsymbol{\gamma}(c^n)|_{k+1,\mathcal{T}_h} + |c^n|_{k+1,\mathcal{T}_h}) + \|c^n - C^n\|_{0,\Omega}\big] \|\boldsymbol{\delta}^n\|_{0,\Omega}.
\end{aligned}$$

- term T_2: Owing to the continuity properties (37) of $\mathcal{A}_h(\cdot;\cdot,\cdot)$ and the interpolation error estimate (51), it holds

$$|T_2| = |\mathcal{A}_h(C^n; \boldsymbol{u}^n - \boldsymbol{u}_I^n, \boldsymbol{\delta}^n)| \le \eta \|\boldsymbol{u}^n - \boldsymbol{u}_I^n\|_{0,\Omega} \|\boldsymbol{\delta}^n\|_{0,\Omega} \le \eta\, h^{k+1} \|\boldsymbol{u}^n\|_{k+1,\mathcal{T}_h} \|\boldsymbol{\delta}^n\|_{0,\Omega}.$$

- term T_3: We have

$$\begin{aligned}
|T_3| &= |\mathcal{A}(c^n; \boldsymbol{u}^n, \boldsymbol{\delta}^n) - \mathcal{A}_h(C^n; \boldsymbol{u}^n, \boldsymbol{\delta}^n)| \\
&\le |(A(c^n)\boldsymbol{u}^n, \boldsymbol{\delta}^n)_{0,\Omega} - (A(\Pi_{k+1}^0 C^n)\boldsymbol{\Pi}_k^{\mathbf{0}} \boldsymbol{u}^n, \boldsymbol{\Pi}_k^{\mathbf{0}} \boldsymbol{\delta}^n)_{0,\Omega}| \\
&\quad + \left| \sum_{K \in \mathcal{T}_h} \nu_{\mathcal{A}}^K(C^n)\, S_{\mathcal{A}}^K((I - \boldsymbol{\Pi}_k^{\mathbf{0},K})\boldsymbol{u}^n, (I - \boldsymbol{\Pi}_k^{\mathbf{0},K})\boldsymbol{\delta}^n) \right| \\
&=: T_3^A + T_3^B.
\end{aligned}$$

  For the term T_3^A, we use Lemma 4.1 with $\kappa = A$, $\sigma = c^n$, $\widehat{\sigma} = C^n$, $\boldsymbol{\chi} = \boldsymbol{u}^n$, $\boldsymbol{\psi} = \boldsymbol{\delta}^n$, $r = k+1$, $s = t = k$, and $m_r = m_s = m_t = k+1$, to get

$$\begin{aligned}
T_3^A \le \eta \Big[& h^{k+1}\big(|A(c^n)\boldsymbol{u}^n|_{k+1,\mathcal{T}_h} + |\boldsymbol{u}^n|_{k+1,\mathcal{T}_h} \|A(c^n)\|_{\infty,\Omega} + |c^n|_{k+1,\mathcal{T}_h} \|\boldsymbol{u}^n\|_{\infty,\Omega}\big) \\
& + \|c^n - C^n\|_{0,\Omega} \|\boldsymbol{u}^n\|_{\infty,\Omega} \Big] \|\boldsymbol{\delta}^n\|_{0,\Omega}.
\end{aligned}$$

  On the other hand, the term T_3^B can be bounded with (32), (6), and Lemma 3.1:

$$T_3^B \le \eta\, h^{k+1} |\boldsymbol{u}^n|_{k+1,\mathcal{T}_h} \|\boldsymbol{\delta}^n\|_{0,\Omega}.$$

After plugging the bounds obtained for T_1–T_3 into (52), dividing by $\|\boldsymbol{\delta}^n\|_{0,\Omega}$, using the triangle inequality in the form

$$\|\boldsymbol{U}^n - \boldsymbol{u}^n\|_{0,\Omega} \le \|\boldsymbol{\delta}^n\|_{0,\Omega} + \|\boldsymbol{u}^n - \boldsymbol{u}_I^n\|_{0,\Omega},$$

and employing (51), the convergence result follows.

The error estimate for the term $\|P^n - p^n\|_{0,\Omega}$ follows easily by combining the above ideas with the argument in [50, Theorem 6.1] and is therefore not shown. □

4.3. Error bounds: concentration

For fixed $\boldsymbol{u}(t) \in \boldsymbol{V}$ and $t \in J$, we define the projector $\mathcal{P}_c : Z \to Z_h$ (that to each $c \in Z$ associates $\mathcal{P}_c c \in Z_h$) by

$$\Gamma_{c,h}(\boldsymbol{u}(t); \mathcal{P}_c c, z_h) = \Gamma_c(\boldsymbol{u}(t); c, z_h), \tag{53}$$

for all $z_h \in Z_h$, where

$$\begin{aligned} \Gamma_{c,h}(\boldsymbol{u}; c, z_h) &:= \mathcal{D}_h(\boldsymbol{u}; c, z_h) + \Theta_h(\boldsymbol{u}; c, z_h) + (c, z_h)_h \\ \Gamma_c(\boldsymbol{u}; c, z_h) &:= \mathcal{D}(\boldsymbol{u}; c, z_h) + \Theta(\boldsymbol{u}; c, z_h) + (c, z_h)_{0,\Omega}, \end{aligned} \tag{54}$$

with

$$(c, z_h)_h := \sum_{K \in \mathcal{T}_h} \int_K c\, (\Pi^{0,K}_{k+1} z_h)\, \mathrm{d}x.$$

Lemma 4.2. *The projector $\mathcal{P}_c : Z \to Z_h$ given in (53) is well-defined under the assumption that $\boldsymbol{u}$, q^+, and q^- are bounded in $L^\infty(\Omega)$ for all $t \in J$.*

Proof. By the Lax–Milgram lemma, we have to show that the left hand side of (53) defines a continuous and coercive bilinear form and that the right hand side is a continuous functional with respect to $\|\cdot\|_{1,\mathcal{T}_h}$. Continuity of the latter one is obtained by combining (14) with

$$\begin{aligned} \Theta(\boldsymbol{u}; c, z_h) + (c, z_h)_{0,\Omega} &= \frac{1}{2}\left[(\boldsymbol{u} \cdot \nabla c, z_h)_{0,\Omega} + ((q^+ + q^- + 2)c, z_h)_{0,\Omega} - (\boldsymbol{u}\, c, \nabla z_h)_{0,\Omega}\right] \\ &\leq \frac{1}{2}\left[\|\boldsymbol{u}\|_{\infty,\Omega}(|c|_{1,\mathcal{T}_h} + \|c\|_{0,\Omega}) + \|q^+ + q^- + 2\|_{\infty,\Omega}\|c\|_{0,\Omega}\right]\|z_h\|_{1,\mathcal{T}_h}. \end{aligned}$$

By using (36) and performing similar computations as in the proof of Lemma 3.3, continuity of $\Gamma_{c,h}$ follows:

$$\Gamma_{c,h}(\boldsymbol{u}; c, z_h) \leq \eta\, \zeta(\boldsymbol{u}, q^+, q^-)\|c\|_{1,\mathcal{T}_h}\|z_h\|_{1,\mathcal{T}_h}, \tag{55}$$

where ζ only depends on the specified functions. Regarding the coercivity of $\Gamma_{c,h}$, we first estimate

$$\Theta_h(\boldsymbol{u}; z_h, z_h) + (z_h, z_h)_h = \sum_{K \in \mathcal{T}_h} \left(\left(\frac{1}{2}(q^+ + q^-) + 1\right)\Pi^{0,K}_{k+1} z_h, \Pi^{0,K}_{k+1} z_h\right)_{0,K} \geq \|\Pi^0_{k+1} z_h\|^2_{0,\Omega},$$

where we recall that $(\Pi^0_{k+1})_{|K} = \Pi^{0,K}_{k+1}$ for all $K \in \mathcal{T}_h$. Then, combining this result with (36) yields

$$\Gamma_{c,h}(\boldsymbol{u}; z_h, z_h) \geq \eta\left[|z_h|^2_{1,\mathcal{T}_h} + \|\Pi^{0,K}_{k+1} z_h\|^2_{0,\Omega}\right] \geq \eta\left[|z_h|^2_{1,\mathcal{T}_h} + \|\overline{z_h}\|^2_{0,\Omega}\right],$$

with $\overline{z_h}$ denoting the $L^2(\Omega)$ projection of z_h onto $\mathbb{P}_0(\Omega)$. Since $\overline{z_h}$ coincides with the average of z_h, one can use a Poincaré–Friedrichs inequality, see e.g. [67], to deduce

$$|z_h|^2_{1,\mathcal{T}_h} + \|\overline{z_h}\|^2_{0,\Omega} \geq C_p^{-1}\mathrm{diam}(\Omega)^{-1}\|z_h\|^2_{1,\mathcal{T}_h},$$

and consequently the coercivity of $\Gamma_{c,h}$. □

Lemma 4.3. *We assume that $\boldsymbol{u} \in [H^{k+1}(\mathcal{T}_h) \cap L^\infty(\Omega)]^2$, $c \in H^{k+2}(\mathcal{T}_h) \cap W^{1,\infty}(\mathcal{T}_h)$, $q^+, q^- \in L^\infty(\Omega)$, $(q^+ + q^-)c \in H^{k+1}(\mathcal{T}_h)$, $\boldsymbol{u}\, c \in [H^{k+1}(\mathcal{T}_h)]^2$, $\boldsymbol{u} \cdot \nabla c \in H^{k+1}(\mathcal{T}_h)$, and $D(\boldsymbol{u})\nabla c \in [H^{k+1}(\mathcal{T}_h)]^2$ for all $t \in J$. Then, the following error bounds for $c - \mathcal{P}_c c$, where $\mathcal{P}_c c$ is defined in (53), hold for all $k \in \mathbb{N}_0$:*

$$\begin{aligned} \|c - \mathcal{P}_c c\|_{1,\mathcal{T}_h} &\leq h^{k+1}\, \xi_1(c, \boldsymbol{u}, q^+, q^-, D(\boldsymbol{u})\nabla c, \nabla c, (q^+ + q^-)c, \boldsymbol{u} \cdot \nabla c, \boldsymbol{u}\, c), \\ \|c - \mathcal{P}_c c\|_{0,\Omega} &\leq h^{k+2}\, \xi_0(c, \boldsymbol{u}, q^+, q^-, D(\boldsymbol{u})\nabla c, \nabla c, (q^+ + q^-)c, \boldsymbol{u} \cdot \nabla c, \boldsymbol{u}\, c), \end{aligned} \tag{56}$$

where the constants $\xi_1, \xi_0 > 0$ only depend on the listed terms and are independent of h.

Proof. We focus on the error estimate in the broken H^1 norm at a fixed time $t \in J$. Firstly, we state the following result. Given $c \in H^{k+2}(\mathcal{T}_h)$, there exists an interpolant $c_I \in Z_h$ such that the following bounds hold true (see for instance [59,60,68]):

$$\|c - c_I\|_{0,\Omega} \leq \eta\, h^{k+2}\|c\|_{k+2,\mathcal{T}_h}, \quad \|c - c_I\|_{1,\mathcal{T}_h} \leq \eta\, h^{k+1}\|c\|_{k+2,\mathcal{T}_h}. \tag{57}$$

After denoting $\nu := \mathcal{P}_c c - c_I$, one obtains with the coercivity of $\Gamma_{c,h}$, see the proof of Lemma 4.2, and the definition of $\mathcal{P}_c c$ in (53),

$$\begin{aligned} M\|\nu\|^2_{1,\mathcal{T}_h} &\le \Gamma_{c,h}(\boldsymbol{u},\nu,\nu) = \Gamma_{c,h}(\boldsymbol{u},\mathcal{P}_c c,\nu) - \Gamma_{c,h}(\boldsymbol{u},c_I,\nu) \\ &= [\Gamma_c(\boldsymbol{u},c,\nu) - \Gamma_{c,h}(\boldsymbol{u},c,\nu)] + \Gamma_{c,h}(\boldsymbol{u},c-c_I,\nu) \\ &=: S_1 + S_2, \end{aligned} \tag{58}$$

for a constant $M > 0$. By employing the definitions of Γ_c and $\Gamma_{c,h}$ in (54), the term S_1 is split as follows:

$$\begin{aligned} S_1 &= [\mathcal{D}(\boldsymbol{u};c,\nu) - \mathcal{D}_h(\boldsymbol{u};c,\nu)] + [\Theta(\boldsymbol{u};c,\nu) - \Theta_h(\boldsymbol{u};c,\nu)] + [(c,\nu)_{0,\Omega} - (c,\nu)_h] \\ &=: S_1^A + S_1^B + S_1^C. \end{aligned}$$

For S_1^A, we have

$$\begin{aligned} S_1^A &= [(D(\boldsymbol{u})\nabla c,\nabla\nu)_{0,\Omega} - (D(\boldsymbol{\Pi}^{\mathbf{0}}_{\boldsymbol{k}}\boldsymbol{u})\,\boldsymbol{\Pi}^{\mathbf{0}}_{\boldsymbol{k}}(\nabla c),\boldsymbol{\Pi}^{\mathbf{0}}_{\boldsymbol{k}}(\nabla\nu))_{0,\Omega}] \\ &\quad + \sum_{K\in\mathcal{T}_h} \nu_D^K(\boldsymbol{u}) S_D^K((I-\Pi^{\nabla,K}_{k+1})c,(I-\Pi^{\nabla,K}_{k+1})\nu) \\ &\le \eta\, h^{k+1}\left[|D(\boldsymbol{u})\nabla c|_{k+1,\mathcal{T}_h} + |\nabla c|_{k+1,\mathcal{T}_h}(\|D(\boldsymbol{u})\|_{\infty,\Omega}+1) + |\boldsymbol{u}|_{k+1,\mathcal{T}_h}\|\nabla c\|_{\infty,\Omega}\right]|\nu|_{1,\mathcal{T}_h}, \end{aligned}$$

where in the inequality we applied Lemma 4.1 to estimate the first part on the right hand side of S_1^A, and made use of the continuity properties (32) of $S_D^K(\cdot,\cdot)$, the trivial continuity property of $\Pi^{\nabla,K}_{k+1}$ in the H^1 seminorm and its approximation properties (stated in Lemma 3.1) to estimate the stabilization term.

Next, for S_1^B, we compute

$$\begin{aligned} S_1^B &= \frac{1}{2}\Big\{ \left[(\boldsymbol{u}\cdot\nabla c,\nu)_{0,\Omega} - (\boldsymbol{\Pi}^{\mathbf{0}}_{\boldsymbol{k}}\boldsymbol{u}\cdot\boldsymbol{\Pi}^{\mathbf{0}}_{\boldsymbol{k}}(\nabla c),\Pi^0_{k+1}\nu)_{0,\Omega}\right] \\ &\quad + \left[((q^+ + q^-)c,\nu)_{0,\Omega} - ((q^+ + q^-)\Pi^0_{k+1}c,\Pi^0_{k+1}\nu)_{0,\Omega}\right] \\ &\quad - \left[(\boldsymbol{u}\,c,\nabla\nu)_{0,\Omega} - (\boldsymbol{\Pi}^{\mathbf{0}}_{\boldsymbol{k}}\boldsymbol{u}\,\Pi^0_{k+1}c,\boldsymbol{\Pi}^{\mathbf{0}}_{\boldsymbol{k}}(\nabla\nu))_{0,\Omega}\right]\Big\} \\ &\le \eta\, h^{k+1}\big[|\boldsymbol{u}\cdot\nabla c|_{k+1,\mathcal{T}_h} + (|\nabla c|_{k+1,\mathcal{T}_h} + |c|_{k+1,\mathcal{T}_h})\|\boldsymbol{u}\|_{\infty,\Omega} + |c|_{k+1,\mathcal{T}_h}\|q^+ + q^-\|_{\infty,\Omega} \\ &\qquad + |(q^+ + q^-)c|_{k+1,\mathcal{T}_h} + |\boldsymbol{u}\,c|_{k+1,\mathcal{T}_h} + |\boldsymbol{u}|_{k+1,\mathcal{T}_h}(\|c\|_{\infty,\Omega} + \|\nabla c\|_{\infty,\Omega})\big]\|\nu\|_{1,\mathcal{T}_h}, \end{aligned}$$

where in the last inequality we used Lemma 4.1 with $\kappa = id$ and $\sigma = \boldsymbol{u}$ for the first and third terms inside the curly bracket, and $\kappa = q^+ + q^-$ and $\sigma = 1$ for the second one.

Finally, for S_1^C, it holds with the definition of the L^2 projector and Lemma 3.1

$$S_1^C = ((I-\Pi^0_{k+1})c,\nu)_{0,\Omega} \le \eta\, h^{k+1}|c|_{k+1,\mathcal{T}_h}\|\nu\|_{0,\Omega}.$$

On the other hand, for S_2, we use the continuity of $\Gamma_{c,h}$ in (55), together with the interpolation error estimate (57), to derive

$$\Gamma_{c,h}(\boldsymbol{u};c-c_I,\nu) \le \eta\,\zeta(\boldsymbol{u},q^+,q^-)\|c-c_I\|_{1,\mathcal{T}_h}\|\nu\|_{1,\mathcal{T}_h} \le \eta\,\zeta(\boldsymbol{u},q^+,q^-)h^{k+1}\|c\|_{k+2,\mathcal{T}_h}\|\nu\|_{1,\mathcal{T}_h}.$$

The error bound in the broken H^1 norm follows by plugging first the estimates for S_1^A, S_1^B, and S_1^C into S_1, then those obtained for S_1 and S_2 into (58), using the definition of the H^1 norm, dividing by $\|\nu\|_{1,\mathcal{T}_h}$, and using the triangle inequality in the form

$$\|c-\mathcal{P}_c c\|_{1,\mathcal{T}_h} \le \|c-c_I\|_{1,\mathcal{T}_h} + \|\nu\|_{1,\mathcal{T}_h},$$

together with the approximation properties (57) of the interpolant c_I.

The L^2 error bound can be derived by combining the above arguments with a standard duality argument as in [20], also recalling the convexity of Ω; it is omitted here. □

By differentiation of (53) in time and use of similar techniques as in the proof of Lemma 4.3, an analogous result can be obtained for $\frac{\partial}{\partial t}(c-\mathcal{P}_c c)$, summarized in the following corollary.

Corollary 1. *Provided that the continuous data and solution are sufficiently regular in space and time, it holds*

$$\left\| \frac{\partial}{\partial t}(c - \mathcal{P}_c c) \right\|_{1,\mathcal{T}_h} \leq h^{k+1}\, \xi_{1,t}, \qquad \left\| \frac{\partial}{\partial t}(c - \mathcal{P}_c c) \right\|_{0,\Omega} \leq h^{k+2}\, \xi_{0,t},$$

where the constants $\xi_{1,t}, \xi_{0,t} > 0$ *are independent of* h.

Moreover, we will later on need the two subsequent bounds.

Lemma 4.4. *Under sufficient smoothness of the continuous data and solution, it holds*

$$\left\| \frac{\partial c^n}{\partial t} - \frac{\mathcal{P}_c c^n - \mathcal{P}_c c^{n-1}}{\tau} \right\|_{0,\Omega} \leq \tau^{\frac{1}{2}} \left\| \frac{\partial^2 c}{\partial s^2} \right\|_{L^2(t_{n-1},t_n;L^2(\Omega))} + \tau^{-\frac{1}{2}} h^{k+2} \left(\int_{t_{n-1}}^{t_n} \xi_{0,t}^2 \, \mathrm{d}s \right)^{\frac{1}{2}},$$

where $\xi_{0,t}$ *can be found in Corollary 1.*

Proof. We estimate

$$\begin{aligned} \left\| \frac{\partial c}{\partial t} - \frac{\mathcal{P}_c c^n - \mathcal{P}_c c^{n-1}}{\tau} \right\|_{0,\Omega} &\leq \left\| \frac{\partial c^n}{\partial t} - \frac{c^n - c^{n-1}}{\tau} \right\|_{0,\Omega} + \left\| \frac{\mathcal{P}_c c^n - \mathcal{P}_c c^{n-1}}{\tau} - \frac{c^n - c^{n-1}}{\tau} \right\|_{0,\Omega} \\ &=: (I) + (II). \end{aligned}$$

The term (I) can be estimated exactly as for standard finite elements, see for instance [69]:

$$(I) = \left\| \frac{\partial c^n}{\partial t} - \frac{c^n - c^{n-1}}{\tau} \right\|_{0,\Omega} \leq \int_{t_{n-1}}^{t_n} \left\| \frac{\partial^2 c}{\partial s^2}(s) \right\|_{0,\Omega} \mathrm{d}s \leq \tau^{\frac{1}{2}} \left(\int_{t_{n-1}}^{t_n} \left\| \frac{\partial^2 c}{\partial s^2}(s) \right\|_{0,\Omega}^2 \mathrm{d}s \right)^{\frac{1}{2}},$$

where we also applied the Hölder inequality in the last step. Concerning (II), this term can be bounded as follows, using Corollary 1:

$$\begin{aligned} (II) &= \left\| \frac{\mathcal{P}_c c^n - \mathcal{P}_c c^{n-1}}{\tau} - \frac{c^n - c^{n-1}}{\tau} \right\|_{0,\Omega} = \frac{1}{\tau} \left\| \int_{t_{n-1}}^{t_n} \frac{\partial}{\partial s}(\mathcal{P}_c c - c)(s) \, \mathrm{d}s \right\|_{0,\Omega} \\ &\leq \tau^{-\frac{1}{2}} \left(\int_{t_{n-1}}^{t_n} \left\| \frac{\partial}{\partial s}(\mathcal{P}_c c - c)(s) \right\|_{0,\Omega}^2 \mathrm{d}s \right)^{\frac{1}{2}} \leq \tau^{-\frac{1}{2}} h^{k+2} \left(\int_{t_{n-1}}^{t_n} \xi_{0,t}^2 \, \mathrm{d}s \right)^{\frac{1}{2}}. \end{aligned}$$

The statement of the lemma follows. □

Lemma 4.5. *Provided that the continuous data and solution are sufficiently regular in space and time, it holds*

$$\|\boldsymbol{u}^n - \boldsymbol{U}^{n-1}\|_{0,\Omega} \leq \tau \left\| \frac{\partial \boldsymbol{u}}{\partial t} \right\|_{L^\infty(t_{n-1},t_n;L^2(\Omega))} + \|C^{n-1} - c^{n-1}\|_{0,\Omega}\, \zeta_1^{n-1} + h^{k+1}\, \zeta_2^{n-1},$$

where ζ_1^{n-1} *and* ζ_2^{n-1} *are the constants from Theorem 1.*

Proof. By using the triangle inequality, one obtains

$$\|\boldsymbol{u}^n - \boldsymbol{U}^{n-1}\|_{0,\Omega} \leq \|\boldsymbol{u}^n - \boldsymbol{u}^{n-1}\|_{0,\Omega} + \|\boldsymbol{u}^{n-1} - \boldsymbol{U}^{n-1}\|_{0,\Omega}.$$

The first term on the right hand side is estimated by

$$\|\boldsymbol{u}^n - \boldsymbol{u}^{n-1}\|_{0,\Omega} = \left\| \int_{t_{n-1}}^{t_n} \frac{\partial \boldsymbol{u}(s)}{\partial s} \, \mathrm{d}s \right\|_{0,\Omega} \leq \tau \left\| \frac{\partial \boldsymbol{u}}{\partial t} \right\|_{L^\infty(t_{n-1},t_n;L^2(\Omega))},$$

and the second one term is bounded with Theorem 1. □

Now, we have all the ingredients to bound $\|c^n - C^n\|_{0,\Omega}$.

Theorem 2. *Let the mesh assumptions **(D1)–(D3)** be satisfied. Then, provided that the continuous data and solutions are sufficiently regular, it yields*

$$\|c^n - C^n\|_{0,\Omega} \leq \eta \left[\|c_{0,h} - c^0\|_{0,\Omega} + h^{k+1}\, \varphi_1 + \tau\, \varphi_2 \right],$$

where the regularity terms φ_1, φ_2 and the positive constant η now depend on $\boldsymbol{u}$, c, q^+, q^-, $\widehat{c}$, $\frac{\partial \boldsymbol{u}}{\partial t}$, $\frac{\partial^2 \boldsymbol{u}}{\partial t^2}$, $\frac{\partial c}{\partial t}$, and $\frac{\partial^2 c}{\partial t^2}$ (and products of these functions).

Proof. We divide the proof intro three steps.

Step 1: writing the basic discrete evolution equation for the error. To start with, we write

$$C^n - c^n = (C^n - \mathcal{P}_c c^n) + (\mathcal{P}_c c^n - c^n) =: \vartheta^n + \rho^n.$$

Eq. (56) gives a bound on ρ^n. In order to deal with ϑ^n, we use the continuous concentration equation (12) with $z = \vartheta^n$, the fully discretized version (45) with $z_h = \vartheta^n$, and the definition of the projector $\mathcal{P}_c c^n$ in (53) with $z_h = \vartheta^n$:

$$\begin{aligned}
&\mathcal{M}_h\left(\frac{\vartheta^n - \vartheta^{n-1}}{\tau}, \vartheta^n\right) + \mathcal{D}_h(\boldsymbol{U}^{n-1}; \vartheta^n, \vartheta^n) \\
&= \left[\mathcal{M}\left(\frac{\partial c^n}{\partial t}, \vartheta^n\right)_{0,\Omega} - \mathcal{M}_h\left(\frac{\mathcal{P}_c c^n - \mathcal{P}_c c^{n-1}}{\tau}, \vartheta^n\right)\right] \\
&\quad + \left[\Theta_h(\boldsymbol{u}^n; \mathcal{P}_c c^n, \vartheta^n) - \Theta_h(\boldsymbol{U}^{n-1}; C^n, \vartheta^n)\right] + \left[\mathcal{D}_h\left(\boldsymbol{u}^n; \mathcal{P}_c c^n, \vartheta^n\right) - \mathcal{D}_h\left(\boldsymbol{U}^{n-1}; \mathcal{P}_c c^n, \vartheta^n\right)\right] \\
&\quad + \left[(\mathcal{P}_c c^n, \vartheta^n)_h - (c^n, \vartheta^n)_{0,\Omega}\right] + \left[((q^+)^n \widehat{c}^n, \vartheta^n)_h - ((q^+)^n \widehat{c}^n, \vartheta^n)_{0,\Omega}\right] \\
&\quad =: R_1 + R_2 + R_3 + R_4 + R_5.
\end{aligned} \tag{59}$$

Owing to the coercivity properties in (36), the second term on the left hand side of (59) can be estimated by

$$\mathcal{D}_h(\boldsymbol{U}^{n-1}; \vartheta^n, \vartheta^n) \geq D_* \left|\vartheta^n\right|^2_{1,\mathcal{T}_h}, \tag{60}$$

with some constant $D_* > 0$ independent of h and $\boldsymbol{U}^{n-1}$.

Step 2: bounding the error terms R_1–R_5. The terms R_1–R_5 on the right hand side of (59) are estimated as follows:

- term R_1: Using the definition of $\mathcal{M}_h(\cdot,\cdot)$ in (25) together with (32) yields

$$\begin{aligned}
R_1 &= \mathcal{M}\left(\frac{\partial c^n}{\partial t}, \vartheta^n\right)_{0,\Omega} - \mathcal{M}_h\left(\frac{\mathcal{P}_c c^n - \mathcal{P}_c c^{n-1}}{\tau}, \vartheta^n\right) \\
&= \left[\left(\phi\, \frac{\partial c^n}{\partial t}, \vartheta^n\right)_{0,\Omega} - \left(\Pi^0_{k+1}\left(\phi\, \Pi^0_{k+1}\left(\frac{\mathcal{P}_c c^n - \mathcal{P}_c c^{n-1}}{\tau}\right)\right), \vartheta^n\right)_{0,\Omega}\right. \\
&\qquad \left. - \sum_{K\in\mathcal{T}_h} \nu^K_{\mathcal{M}}(\phi) S^K_{\mathcal{M}}\left((I - \Pi^{0,K}_{k+1})\left(\frac{\mathcal{P}_c c^n - \mathcal{P}_c c^{n-1}}{\tau}\right), (I - \Pi^{0,K}_{k+1})\vartheta^n\right)\right] \\
&\leq \eta\left[\left\|\phi\, \frac{\partial c^n}{\partial t} - \Pi^0_{k+1}\left(\phi\, \Pi^0_{k+1}\left(\frac{\mathcal{P}_c c^n - \mathcal{P}_c c^{n-1}}{\tau}\right)\right)\right\|_{0,\Omega}\right. \\
&\qquad \left. + \left\|(I - \Pi^0_{k+1})\left(\frac{\mathcal{P}_c c^n - \mathcal{P}_c c^{n-1}}{\tau}\right)\right\|_{0,\Omega}\right] \|\vartheta^n\|_{0,\Omega} \\
&=: \eta[R_1^A + R_1^B]\|\vartheta^n\|_{0,\Omega}.
\end{aligned}$$

The term R_1^A is estimated by using the continuity of the L^2 projector, the assumption (6) on ϕ, and the approximation properties in Lemma 3.1:

$$\begin{aligned} R_1^A &\le \left\| (I - \Pi^0_{k+1}) \left(\phi \frac{\partial c^n}{\partial t} \right) \right\|_{0,\Omega} + \left\| \Pi^0_{k+1} \left(\phi \frac{\partial c^n}{\partial t} - \phi\, \Pi^0_{k+1} \left(\frac{\partial c^n}{\partial t} \right) \right) \right\|_{0,\Omega} \\ &\quad + \left\| \Pi^0_{k+1} \left(\phi\, \Pi^0_{k+1} \left(\frac{\partial c^n}{\partial t} - \frac{\mathcal{P}_c c^n - \mathcal{P}_c c^{n-1}}{\tau} \right) \right) \right\|_{0,\Omega} \\ &\le \eta \left[h^{k+2} \left(\left| \phi \frac{\partial c^n}{\partial t} \right|_{k+2,\mathcal{T}_h} + \left| \frac{\partial c^n}{\partial t} \right|_{k+2,\mathcal{T}_h} \right) + \left\| \frac{\partial c^n}{\partial t} - \frac{\mathcal{P}_c c^n - \mathcal{P}_c c^{n-1}}{\tau} \right\|_{0,\Omega} \right]. \end{aligned}$$

Next, we estimate R_1^B with similar tools as for R_1^A:

$$\begin{aligned} R_1^B &\le \left\| (I - \Pi^0_{k+1}) \left(\frac{\mathcal{P}_c c^n - \mathcal{P}_c c^{n-1}}{\tau} - \frac{\partial c^n}{\partial t} \right) \right\|_{0,\Omega} + \left\| (I - \Pi^0_{k+1}) \frac{\partial c^n}{\partial t} \right\|_{0,\Omega} \\ &\le \left\| \frac{\mathcal{P}_c c^n - \mathcal{P}_c c^{n-1}}{\tau} - \frac{\partial c^n}{\partial t} \right\|_{0,\Omega} + \eta\, h^{k+2} \left| \frac{\partial c^n}{\partial t} \right|_{k+2,\mathcal{T}_h}. \end{aligned}$$

Thus, we deduce with Lemma 4.4

$$\begin{aligned} R_1 &\le \eta \left[h^{k+2} \left(\left| \phi \frac{\partial c^n}{\partial t} \right|_{k+2,\mathcal{T}_h} + \left| \frac{\partial c^n}{\partial t} \right|_{k+2,\mathcal{T}_h} \right) + \tau^{-\frac{1}{2}} h^{k+2} \left(\int_{t_{n-1}}^{t_n} \xi_{0,t}^2 \, \mathrm{d}s \right)^{\frac{1}{2}} \right. \\ &\quad \left. + \tau^{\frac{1}{2}} \left\| \frac{\partial^2 c}{\partial s^2} \right\|_{L^2(t_{n-1},t_n;L^2(\Omega))} \right] \|\vartheta^n\|_{0,\Omega} \\ &=: \left[h^{k+2} R_1^{n,1} + \tau^{-\frac{1}{2}} h^{k+2} R_1^{n,2} + \tau^{\frac{1}{2}} R_1^{n,3} \right] \|\vartheta^n\|_{0,\Omega}, \end{aligned} \tag{61}$$

with the obvious definitions for the regularity terms $R_1^{n,1}$, $R_1^{n,2}$, and $R_1^{n,3}$.

- term R_2: By the definition of $\Theta_h(\cdot;\cdot,\cdot)$ in (27), the identity $\vartheta^n = C^n - \mathcal{P}_c c^n$, and the fact that $(q^+)^n$ and $(q^-)^n$ are non-negative, it holds

$$\begin{aligned} &\Theta_h(\boldsymbol{u}^n; \mathcal{P}_c c^n, \vartheta^n) - \Theta_h(\boldsymbol{U}^{n-1}; C^n, \vartheta^n) \\ &= \frac{1}{2} \left[\left(\boldsymbol{u}^n \cdot \nabla \mathcal{P}_c c^n, \vartheta^n \right)_h - \left(\boldsymbol{U}^{n-1} \cdot \nabla C^n, \vartheta^n \right)_h \right] - \frac{1}{2} \left((q^+ + q^-)\vartheta^n, \vartheta^n \right)_{0,\Omega} \\ &- \frac{1}{2} \left[\left(\boldsymbol{u}^n \mathcal{P}_c c^n, \nabla \vartheta^n \right)_h - \left(\boldsymbol{U}^{n-1} C^n, \nabla \vartheta^n \right)_h \right] \\ &\le \frac{1}{2} \left[\left(\boldsymbol{u}^n \cdot \nabla \mathcal{P}_c c^n, \vartheta^n \right)_h - \left(\boldsymbol{U}^{n-1} \cdot \nabla C^n, \vartheta^n \right)_h - \left(\boldsymbol{u}^n \mathcal{P}_c c^n, \nabla \vartheta^n \right)_h + \left(\boldsymbol{U}^{n-1} C^n, \nabla \vartheta^n \right)_h \right]. \end{aligned}$$

The above equation, after adding zero in the form

$$\begin{aligned} 0 &= (\boldsymbol{U}^{n-1} \cdot \nabla \vartheta^n, \vartheta^n)_h - (\boldsymbol{U}^{n-1} \cdot \nabla \vartheta^n, \vartheta^n)_h \\ &= (\boldsymbol{U}^{n-1} \cdot \nabla C^n, \vartheta^n)_h - (\boldsymbol{U}^{n-1} \cdot \nabla \mathcal{P}_c c^n, \vartheta^n)_h - (\boldsymbol{U}^{n-1} \cdot \nabla \vartheta^n, C^n)_h + (\boldsymbol{U}^{n-1} \cdot \nabla \vartheta^n, \mathcal{P}_c c^n)_h \end{aligned}$$

to the right hand side, can be equivalently expressed as

$$\begin{aligned} &\Theta_h(\boldsymbol{u}^n; \mathcal{P}_c c^n, \vartheta^n) - \Theta_h(\boldsymbol{U}^{n-1}; C^n, \vartheta^n) \\ &\le \frac{1}{2} \left[\left((\boldsymbol{u}^n - \boldsymbol{U}^{n-1}) \cdot \nabla \mathcal{P}_c c^n, \vartheta^n \right)_h - \left((\boldsymbol{u}^n - \boldsymbol{U}^{n-1}) \mathcal{P}_c c^n, \nabla \vartheta^n \right)_h \right] =: R_2^A + R_2^B. \end{aligned}$$

For R_2^A, we estimate

$$R_2^A = \frac{1}{2} \left((\boldsymbol{u}^n - \boldsymbol{U}^{n-1}) \nabla \mathcal{P}_c c^n, \vartheta^n \right)_h \le \frac{1}{2} \|\boldsymbol{u}^n - \boldsymbol{U}^{n-1}\|_{0,\Omega} \|\boldsymbol{\Pi}^{\mathbf{0}}_{\boldsymbol{k}} \nabla \mathcal{P}_c c^n\|_{\infty,\Omega} \|\vartheta^n\|_{0,\Omega}.$$

We now use an inverse estimate [65, Lemma 4.5.3], the continuity of $\boldsymbol{\Pi}_k^{\mathbf{0},K}$, a triangle inequality, the assumption that $\mathcal{T}_h$ is quasi-regular, and Lemma 4.3, to deduce, for every $K \in \mathcal{T}_h$,

$$\begin{aligned}
&\|\boldsymbol{\Pi}_k^{\mathbf{0},K}\nabla\mathcal{P}_c c^n\|_{\infty,K} \le \eta\, h_K^{-1}\|\boldsymbol{\Pi}_k^{\mathbf{0},K}\nabla\mathcal{P}_c c^n\|_{0,K} \le \eta\, h_K^{-1}\|\nabla\mathcal{P}_c c^n\|_{0,K}\\
&\quad\le \eta\, h_K^{-1}\left(\|\nabla\mathcal{P}_c c^n - \nabla c^n\|_{0,K} + \|\nabla c^n\|_{0,K}\right)\\
&\quad\le \eta\,\left(h^{-1}\|\nabla\mathcal{P}_c c^n - \nabla c^n\|_{0,\mathcal{T}_h} + \|\nabla c^n\|_{\infty,K}\right) \le \eta.
\end{aligned} \tag{62}$$

Recalling Lemma 4.5, the definitions of ϑ^{n-1} and ρ^{n-1}, and Lemma 4.3, we get

$$\begin{aligned}
&\|\boldsymbol{u}^n - \boldsymbol{U}^{n-1}\|_{0,\Omega}\\
&\quad\le \tau\,\|\partial\boldsymbol{u}/\partial t\|_{L^\infty(t_{n-1},t_n;L^2(\Omega))} + (\|\vartheta^{n-1}\|_{0,\Omega} + \|\rho^{n-1}\|_{0,\Omega})\zeta_1^{n-1} + h^{k+1}\,\zeta_2^{n-1}\\
&\quad\le \tau\,\|\partial\boldsymbol{u}/\partial t\|_{L^\infty(t_{n-1},t_n;L^2(\Omega))} + (\|\vartheta^{n-1}\|_{0,\Omega} + h^{k+2}\xi_0^{n-1})\zeta_1^{n-1} + h^{k+1}\,\zeta_2^{n-1},
\end{aligned} \tag{63}$$

thus implying

$$R_2^A \le \eta\left[h^{k+1}R_2^{n,1} + \tau\,R_2^{n,2} + \|\vartheta^{n-1}\|_{0,\Omega}R_2^{n,3}\right]\|\vartheta^n\|_{0,\Omega},$$

with the obvious definitions for the regularity terms $R_2^{n,1}$, $R_2^{n,2}$, and $R_2^{n,3}$.
The term R_2^B can be bounded analogously to R_2^A, giving

$$R_2^B = \frac{1}{2}\left((\boldsymbol{U}^{n-1} - \boldsymbol{u}^n)\mathcal{P}_c c^n, \nabla\vartheta^n\right)_h \le \eta\,\|\boldsymbol{u}^n - \boldsymbol{U}^{n-1}\|_{0,\Omega}|\vartheta^n|_{1,\mathcal{T}_h}.$$

Using again the bound (63), one obtains

$$R_2^B \le \eta\left[h^{k+1}R_2^{n,1} + \tau\,R_2^{n,2} + \|\vartheta^{n-1}\|_{0,\Omega}R_2^{n,3}\right]|\vartheta^n|_{1,\mathcal{T}_h}.$$

Thus,

$$R_2 \le \eta\left[h^{k+1}R_2^{n,1} + \tau\,R_2^{n,2} + \|\vartheta^{n-1}\|_{0,\Omega}R_2^{n,3}\right]\left(\|\vartheta^n\|_{0,\Omega} + |\vartheta^n|_{1,\mathcal{T}_h}\right).$$

- term R_3: We use the definition of $\mathcal{D}_h(\cdot;\cdot,\cdot)$ in (28), a standard Hölder inequality in the spirit of (15), the estimate (62), the scaling properties of the stabilization in (32), the Lipschitz continuity of $D(\cdot;\cdot,\cdot)$, and ν_D^K in (34), to deduce

$$\begin{aligned}
R_3 &= \mathcal{D}_h\left(\boldsymbol{u}^n;\mathcal{P}_c c^n,\vartheta^n\right) - \mathcal{D}_h\left(\boldsymbol{U}^{n-1};\mathcal{P}_c c^n,\vartheta^n\right)\\
&= ((D(\boldsymbol{\Pi}_k^{\mathbf{0}}\boldsymbol{u}^n) - D(\boldsymbol{\Pi}_k^{\mathbf{0}}\boldsymbol{U}^{n-1}))\,\boldsymbol{\Pi}_k^{\mathbf{0}}(\nabla\mathcal{P}_c c^n)\cdot\boldsymbol{\Pi}_k^{\mathbf{0}}(\nabla\vartheta^n))_{0,\Omega}\\
&\quad + \sum_{K\in\mathcal{T}_h}(\nu_D^K(\boldsymbol{u}^n) - \nu_D^K(\boldsymbol{U}^{n-1}))S_D^K\left((I - \Pi_{k+1}^{\nabla,K})\mathcal{P}_c c^n, (I - \Pi_{k+1}^{\nabla,K})\vartheta^n\right)\\
&\le \eta\|\boldsymbol{u}^n - \boldsymbol{U}^{n-1}\|_{0,\Omega}|\vartheta^n|_{1,\mathcal{T}_h}.
\end{aligned}$$

Hence, with (63) we have

$$R_3 \le \eta\left[h^{k+1}R_2^{n,1} + \tau\,R_2^{n,2} + \|\vartheta^{n-1}\|_{0,\Omega}R_2^{n,3}\right]|\vartheta^n|_{1,\mathcal{T}_h}.$$

- term R_4: The use of Lemma 4.3 yields

$$\begin{aligned}
R_4 &= -[(c^n,\vartheta^n)_{0,\Omega} - (\mathcal{P}_c c^n,\vartheta^n)_h] = -[((I - \Pi_{k+1}^0)c^n,\vartheta^n)_{0,\Omega} + (\Pi_{k+1}^0(c^n - \mathcal{P}_c c^n),\vartheta^n)_{0,\Omega}]\\
&\le \eta\,h^{k+2}\left[|c^n|_{k+2,\mathcal{T}_h} + \xi_0^n\right]\|\vartheta^n\|_{0,\Omega} =: \eta\,h^{k+2}R_4^{n,1}\|\vartheta^n\|_{0,\Omega}
\end{aligned}$$

with the obvious definition of $R_4^{n,1}$.
- term R_5: The approximation properties in Lemma 3.1 yield

$$R_5 = -\left((I - \Pi_{k+1}^0)((q^+)^n\widehat{c}^n),\vartheta^n\right)_{0,\Omega} \le \eta\,h^{k+2}\,|(q^+)^n\widehat{c}^n|_{k+2,\mathcal{T}_h}\|\vartheta^n\|_{0,\Omega} =: \eta\,h^{k+2}R_5^{n,1}\|\vartheta^n\|_{0,\Omega}$$

with the obvious definition of $R_5^{n,1}$.

Step 3: deriving the error estimate at each generic nth time step. We now insert (60) and the bounds on R_1–R_5 into (59). Afterwards, we observe that all regularity terms $\{R_J^{n,i}\}$ above only depend on the continuous solution and can be assumed to be bounded uniformly in h. We only keep track of the terms $R_1^{n,2}$ and $R_1^{n,3}$. This yields

$$\begin{aligned}
&\frac{1}{\tau}\mathcal{M}_h\left(\vartheta^n-\vartheta^{n-1},\vartheta^n\right)+D_*\left|\vartheta^n\right|_{1,\mathcal{T}_h}^2\\
&\leq \|\vartheta^{n-1}\|_{0,\Omega}\|\vartheta^n\|_{0,\Omega}\,\omega_1^n+\|\vartheta^{n-1}\|_{0,\Omega}|\vartheta^n|_{1,\mathcal{T}_h}\omega_2^n+\|\vartheta^n\|_{0,\Omega}\omega_3^n+|\vartheta^n|_{1,\mathcal{T}_h}\omega_4^n\\
&=\|\vartheta^n\|_{0,\Omega}\left[\omega_3^n+\|\vartheta^{n-1}\|_{0,\Omega}\,\omega_1^n\right]+|\vartheta^n|_{1,\mathcal{T}_h}\left[\omega_4^n+\|\vartheta^{n-1}\|_{0,\Omega}\,\omega_2^n\right],
\end{aligned}\tag{64}$$

with the positive scalars

$$\omega_i^n\leq\eta,\quad i=1,2,\quad \omega_3^n\leq\eta\left(\tau+h^{k+1}+\tau^{-\frac{1}{2}}h^{k+2}R_1^{n,2}+\tau^{\frac{1}{2}}R_1^{n,3}\right),\quad \omega_4^n\leq\eta\left(\tau+h^{k+1}\right).\tag{65}$$

Next, we introduce, for all $w_h\in Z_h$, the discrete norm

$$\|w_h\|_{0,h}^2:=\mathcal{M}_h(w_h,w_h).\tag{66}$$

Owing to Lemma 3.2, there exist positive constants c_* and c^*, such that, for all $w_h\in Z_h$, it holds

$$c_*\|w_h\|_{0,h}\leq\|w_h\|_{0,\Omega}\leq c^*\|w_h\|_{0,h}.\tag{67}$$

Reshaping (64), and employing (66) and (67), then gives

$$\begin{aligned}
&\|\vartheta^n\|_{0,h}^2+\tau D_*\left|\vartheta^n\right|_{1,\mathcal{T}_h}^2\\
&\leq\mathcal{M}_h(\vartheta^{n-1},\vartheta^n)+\tau\|\vartheta^n\|_{0,h}\left[c^*\omega_3^n+\|\vartheta^{n-1}\|_{0,h}(c^*)^2\omega_1^n\right]+\tau|\vartheta^n|_{1,\mathcal{T}_h}\left[\omega_4^n+\|\vartheta^{n-1}\|_{0,h}\,c^*\omega_2^n\right]\\
&=:T_1+T_2+T_3.
\end{aligned}\tag{68}$$

The terms T_1 and T_2 are bounded as follows:

$$\begin{aligned}
T_1+T_2&\leq\|\vartheta^n\|_{0,h}\left[(1+\tau\eta)\|\vartheta^{n-1}\|_{0,h}+\tau c^*\omega_3^n\right]\\
&\leq\frac{1}{2}\left(\|\vartheta^n\|_{0,h}^2+\left[(1+\tau\eta)\|\vartheta^{n-1}\|_{0,h}+\tau c^*\omega_3^n\right]^2\right),
\end{aligned}\tag{69}$$

where we used (39) and (66) in the first step. The term T_3 is bounded as follows:

$$\begin{aligned}
T_3&\leq\tau D_*|\vartheta^n|_{1,\mathcal{T}_h}^2+\frac{\tau}{4D_*}\left[\omega_4^n+\|\vartheta^{n-1}\|_{0,h}\,c^*\omega_2^n\right]^2\\
&\leq\tau D_*|\vartheta^n|_{1,\mathcal{T}_h}^2+\frac{\tau}{2}\eta\left[(\omega_4^n)^2+\|\vartheta^{n-1}\|_{0,h}^2\right]^2.
\end{aligned}\tag{70}$$

Next, we plug (69) and (70) into (68), cancel the terms $\tau D_*|\vartheta^n|_{1,\mathcal{T}_h}^2$, and manipulate the resulting inequality, to obtain

$$\|\vartheta^n\|_{0,h}^2\leq\left[(1+\tau\eta)\|\vartheta^{n-1}\|_{0,h}+\tau c^*\omega_3^n\right]^2+\tau\eta\left[(\omega_4^n)^2+\|\vartheta^{n-1}\|_{0,h}^2\right]^2.$$

Moreover, we estimate

$$\begin{aligned}
&\left[(1+\tau\eta)\|\vartheta^{n-1}\|_{0,h}+\tau c^*\omega_3^n\right]^2\\
&\quad=(1+\tau\eta)^2\|\vartheta^{n-1}\|_{0,h}^2+2\tau^{\frac{1}{2}}\|\vartheta^{n-1}\|_{0,h}\tau^{\frac{1}{2}}(1+\tau\eta)c^*\omega_3^n+\tau^2(c^*)^2(\omega_3^n)^2\\
&\quad\leq\left[(1+\tau\eta)^2+\tau\right]\|\vartheta^{n-1}\|_{0,h}^2+\left[\tau(1+\tau\eta)^2+\tau^2\right](c^*)^2(\omega_3^n)^2\\
&\quad\leq(1+\tau\eta)\,\|\vartheta^{n-1}\|_{0,h}^2+\tau\eta(\omega_3^n)^2.
\end{aligned}$$

Hence,

$$\|\vartheta^n\|_{0,h}^2\leq(1+\tau\eta)\|\vartheta^{n-1}\|_{0,h}^2+\tau\eta\left[(\omega_3^n)^2+(\omega_4^n)^2\right].$$

Defining

$$\gamma^n:=(\omega_3^n)^2+(\omega_4^n)^2$$

and solving the recursion then leads to

$$\|\vartheta^n\|_{0,h}^2\leq(1+\tau\eta)^n\|\vartheta^0\|_{0,h}^2+\tau\eta\sum_{j=1}^n\gamma^j\leq\eta\|\vartheta^0\|_{0,h}^2+\tau\eta\sum_{j=1}^n\gamma^j,$$

where we recall that $n \leq T/\tau$ with T the final time instant. With (67) the estimate in the L^2 norm is a direct consequence:

$$\|\vartheta^n\|_{0,\Omega}^2 \leq \eta \|\vartheta^0\|_{0,\Omega}^2 + \tau\eta \sum_{j=1}^{n} \gamma^j. \tag{71}$$

The initial term $\|\vartheta^0\|_{0,\Omega}^2$ is estimated by

$$\|\vartheta^0\|_{0,\Omega} = \|c_{0,h} - \mathcal{P}_c c^0\|_{0,\Omega} \leq \|c_{0,h} - c^0\|_{0,\Omega} + \|c^0 - \mathcal{P}_c c^0\|_{0,\Omega} \leq \|c_{0,h} - c^0\|_{0,\Omega} + h^{k+2}\,\xi_0^0, \tag{72}$$

where we applied Lemma 4.3. Moreover, using (65), the fact that $\sum_{j=1}^{n} \tau \leq T$, and the definitions of $R_1^{j,2}$ and $R_1^{j,3}$ in (61), after some simple manipulations, we obtain

$$\begin{aligned}
\tau\eta \sum_{j=1}^{n} \gamma_j &\leq \eta \left(\sum_{j=1}^{n} \tau(\omega_3^j)^2 + \sum_{j=1}^{n} \tau(\omega_4^j)^2 \right) \\
&\leq \eta \left[\sum_{j=1}^{n} \tau(\tau + h^{k+1})^2 + (h^{k+2})^2 \sum_{j=1}^{n} (R_1^{j,2})^2 + \tau^2 \sum_{j=1}^{n} (R_1^{j,3})^2 \right] \\
&\leq \eta \left[(\tau + h^{k+1})^2 + (h^{k+2})^2 \sum_{j=1}^{n} (R_1^{j,2})^2 + \tau^2 \sum_{j=1}^{n} (R_1^{j,3})^2 \right] \\
&\leq \eta \left[(\tau + h^{k+1})^2 + (h^{k+2})^2 \int_0^{t_n} \xi_{0,t}^2 \,\mathrm{d}s + \tau^2 \int_0^{t_n} \left\| \frac{\partial^2 c}{\partial s^2}(s) \right\|_{0,\Omega}^2 \mathrm{d}s \right].
\end{aligned} \tag{73}$$

The assertion of the theorem follows by combining (71) with (73) and (72). □

5. Numerical experiments

In this section, we demonstrate the performance of the method on the basis of numerical experiments, focusing on the lowest order case $k = 0$ which is expected to be the preferable one for practical application. To this purpose, we firstly consider an ideal test case (Example 1), then we explore the potential of VEM for locally refined meshes (Example 2), and finally we discuss a more realistic test case (Example 3). The aim of the first test is to validate (also numerically) the convergence of the method on a problem with regular known solution, the goal of the second test is to assess the VEM technology for meshes with many hanging nodes and edges with different size, and the idea behind the third test is to check the method's performance on a well-known benchmark that mimics a more realistic situation.

Example 1. Here, we study a generalized version of (1), given by

$$\begin{cases} \phi \dfrac{\partial c}{\partial t} + \boldsymbol{u} \cdot \nabla c - \operatorname{div}(D(\boldsymbol{u})\nabla c) = f \\ \operatorname{div} \boldsymbol{u} = g \\ \boldsymbol{u} = -a(c)(\nabla p - \boldsymbol{\gamma}(c)), \end{cases} \tag{74}$$

endowed with the boundary and initial conditions in (4) and (5), respectively. We fix $\Omega = (0, 1)^2$ and pick the same choice of parameters as in [51], namely $T = 0.01$, $\phi = 1$, $D(\boldsymbol{u}) = |\boldsymbol{u}| + 0.02$, $d_m = 0.02$, $d_\ell = d_t = 1$, $c_0 = 0$, $\boldsymbol{\gamma}(c) = 0$, and $a(c) = (c + 2)^{-1}$, where f and g are taken in accordance with the analytical solutions

$$\begin{aligned}
c(x, y, t) &= t^2 \left[x^2(x-1)^2 + y^2(y-1)^2 \right] \\
\boldsymbol{u}(x, y, t) &= 2t^2 \begin{pmatrix} x(x-1)(2x-1) \\ y(y-1)(2y-1) \end{pmatrix} \\
p(x, y, t) &= -\frac{1}{2}c^2 - 2c + \frac{17}{6300}t^4 + \frac{2}{15}t^2.
\end{aligned} \tag{75}$$

Plots of the exact solution at the final time T are shown in Figs. 1 and 2.

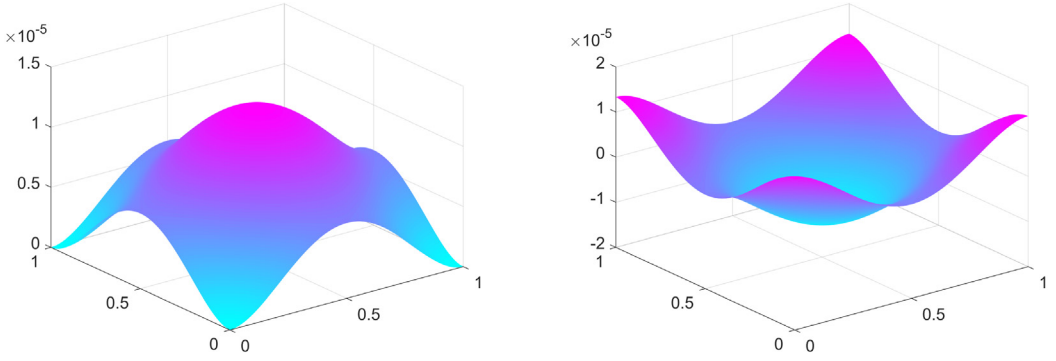

Fig. 1. Example 1. Exact concentration c (left) and pressure p (right) of Example 1, given by (75), at the final time $T = 0.01$.

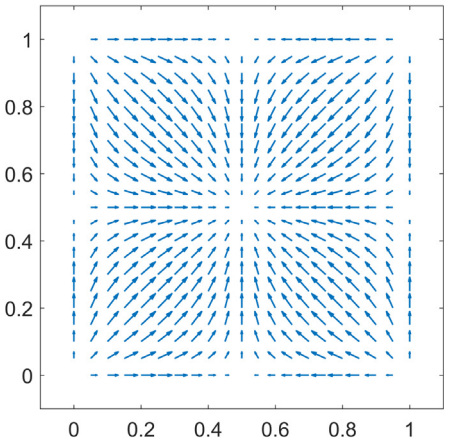

Fig. 2. Example 1. Exact vector field $\boldsymbol{u}$ given by (75), at the final time $T = 0.01$.

We employ a sequence of regular Cartesian meshes and Voronoi meshes, as portrayed in Fig. 3. In addition to the current version, we also test the method when replacing the stabilization terms in (26), (29), and (31) by alternative ones:

$$
\begin{aligned}
\nu^K_{\mathcal{M}}(\phi) S^K_{\mathcal{M}}\left((I-\Pi^{0,K}_{k+1})c_h,(I-\Pi^{0,K}_{k+1})z_h\right) \quad &\rightsquigarrow \quad \widetilde{S^K_{\mathcal{M}}}\left((I-\Pi^{0,K}_{k+1})c_h,(I-\Pi^{0,K}_{k+1})z_h\right)\\
\nu^K_{D}(\boldsymbol{u}_h) S^K_{D}\left((I-\Pi^{\nabla,K}_{k+1})c_h,(I-\Pi^{\nabla,K}_{k+1})z_h\right) \quad &\rightsquigarrow \quad \widetilde{S^K_{D}}\left(\boldsymbol{u}_h;(I-\Pi^{\nabla,K}_{k+1})c_h,(I-\Pi^{\nabla,K}_{k+1})z_h\right)\\
\nu^K_{\mathcal{A}}(c_h) S^K_{\mathcal{A}}\left((I-\boldsymbol{\Pi}^{\boldsymbol{0},\boldsymbol{K}}_{\boldsymbol{k}})\boldsymbol{u}_h,(I-\boldsymbol{\Pi}^{\boldsymbol{0},\boldsymbol{K}}_{\boldsymbol{k}})\boldsymbol{v}_h\right) \quad &\rightsquigarrow \quad \widetilde{S^K_{\mathcal{A}}}\left(c_h;(I-\boldsymbol{\Pi}^{\boldsymbol{0},\boldsymbol{K}}_{\boldsymbol{k}})\boldsymbol{u}_h,(I-\boldsymbol{\Pi}^{\boldsymbol{0},\boldsymbol{K}}_{\boldsymbol{k}})\boldsymbol{v}_h\right).
\end{aligned}
$$

The alternative (diagonal) stabilizations are given by

$$
\begin{aligned}
\widetilde{S^K_{\mathcal{M}}}(c_h,z_h) &= |K| \sum_{j=1}^{\dim Z_h(K)} d^{\mathcal{M}}_j \,\mathrm{dof}^{Z_h(K)}_j(c_h)\,\mathrm{dof}^{Z_h(K)}_j(z_h)\\
\widetilde{S^K_{D}}(c_h,z_h) &= \sum_{j=1}^{\dim Z_h(K)} d^{D}_j \,\mathrm{dof}^{Z_h(K)}_j(c_h)\,\mathrm{dof}^{Z_h(K)}_j(z_h)\\
\widetilde{S^K_{\mathcal{A}}}(\boldsymbol{u}_h,\boldsymbol{v}_h) &= |K| \sum_{j=1}^{\dim \boldsymbol{V}_h(K)} d^{\mathcal{A}}_j \,\mathrm{dof}^{\boldsymbol{V}_h(K)}_j(\boldsymbol{u}_h)\,\mathrm{dof}^{\boldsymbol{V}_h(K)}_j(\boldsymbol{v}_h),
\end{aligned}
\tag{76}
$$

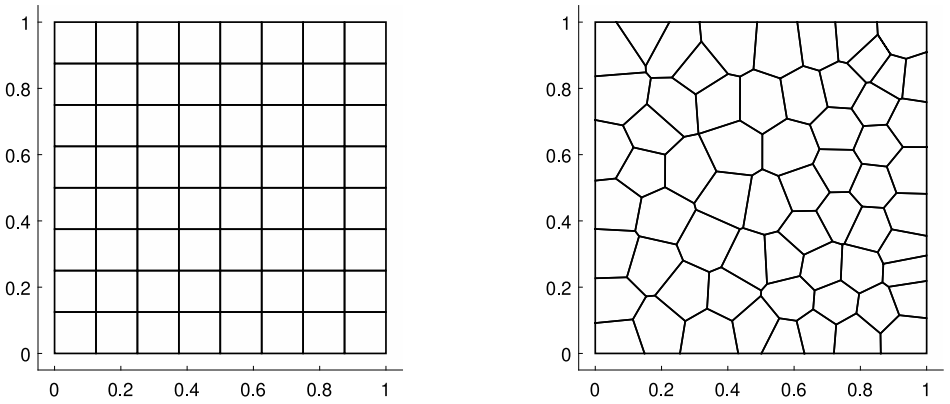

Fig. 3. Example 1. Meshes: regular 8×8 Cartesian mesh (left); Voronoi mesh with 64 elements (right).

with

$$
\begin{aligned}
d_j^{\mathcal{M}} &:= \max\left\{ \frac{1}{|K|} \int_K \phi\, (\Pi_{k+1}^{0,K} \varphi_j^K)^2 \,\mathrm{d}x,\ \sigma\, \nu_{\mathcal{M}}^K(\phi) \right\} \\
d_j^{D} &:= \max\left\{ \int_K D(\boldsymbol{\Pi}_{\boldsymbol{k}}^{\boldsymbol{0},\boldsymbol{K}} \boldsymbol{u}_h)\, |\boldsymbol{\Pi}_{\boldsymbol{k}}^{\boldsymbol{0},\boldsymbol{K}} (\nabla \varphi_j^K)|^2 \,\mathrm{d}x,\ \sigma\, \nu_D^K(\boldsymbol{u}_h) \right\} \\
d_j^{\mathcal{A}} &:= \max\left\{ \frac{1}{|K|} \int_K A(\Pi_{k+1}^{0,K} c_h)\, |\boldsymbol{\Pi}_{\boldsymbol{k}}^{\boldsymbol{0},\boldsymbol{K}} \boldsymbol{\psi}_j^K|^2 \,\mathrm{d}x,\ \sigma\, \nu_{\mathcal{A}}^K(c_h) \right\},
\end{aligned}
\tag{77}
$$

where $\{\varphi_j^K\}_{\ell=1}^{\dim Z_h(K)}$ and $\{\boldsymbol{\psi}_j^K\}_{\ell=1}^{\dim \boldsymbol{V}_h(K)}$ denote the local canonical basis functions for $Z_h(K)$ and $\boldsymbol{V}_h(K)$, and $\sigma > 0$ is a safety parameter. In the forthcoming experiments, we set $\sigma = 1e{-}3$. We highlight that these stabilizations are in fact modifications of the so-called *D-recipe*, which was introduced in [3] and has already been successfully applied in some variants to other model problems, such as the Helmholtz problem [14]. The first entry inside the max is simply the "diagonal part" of the consistency term of the local approximate forms in (26), (29), and (31), respectively, whereas the second terms correspond to the original stabilizations associated to the degrees of freedom in (33) multiplied by σ, which acts as a positivity safeguard. Importantly, it is easy to check that the error analysis can be easily extended to the new choice of stabilizations.

Due to the virtuality of the basis functions, we measure the following relative L^2 errors:

$$
\frac{\|c - \Pi_1^0 C^n\|_{0,\Omega}}{\|c\|_{0,\Omega}}, \qquad \frac{\|\boldsymbol{u} - \boldsymbol{\Pi}_0^0 \boldsymbol{U}^n\|_{0,\Omega}}{\|\boldsymbol{U}^n\|_{0,\Omega}}, \qquad \frac{\|p - \Pi_0^0 P^n\|_{0,\Omega}}{\|p\|_{0,\Omega}},
$$

where C^n, $\boldsymbol{U}^n$, and P^n are the numerical solutions at the final time T.

The relative L^2 discretization errors for the concentration are plotted in Fig. 4 in terms of the mesh size h for both families of meshes and both variants of stabilizations. In order to better underline the expected linear convergence of the method both in h and τ (see Theorem 2, recalling that $k = 0$), the time step τ is chosen proportional to h. In other words, starting with the coarsest mesh and $\tau = T/5$, each subsequent case is obtained by dividing both h (adopting a finer mesh) and τ by a factor of 2. Analogous plots are shown for the velocity and pressure variable errors in Figs. 5 and 6. In all cases, the linear convergence rates are in accordance with Theorems 1 and 2. For the pressure discretization error, since the initial meshes are very coarse, we observe some pre-asymptotic regime when employing the original stabilizations in (33). This effect, however, is not present for the alternative stabilizations in (76). Both variants lead to similar results for the concentration and velocity errors.

Since the concentration often evolves more rapidly than the velocity and pressure, it could be worth to consider a cheaper variant of the discrete scheme (44)–(46) where the discrete velocity–pressure pair is updated only every R time step (with $R \in \mathbb{N}$). This leads to a smaller number of linear system resolutions (possibly with a small reduction in accuracy) since only system (45) is solved at every time step, while (46) is solved only every R step. In order to test this, we tried to run the same test above and compare the original version with the cheaper version

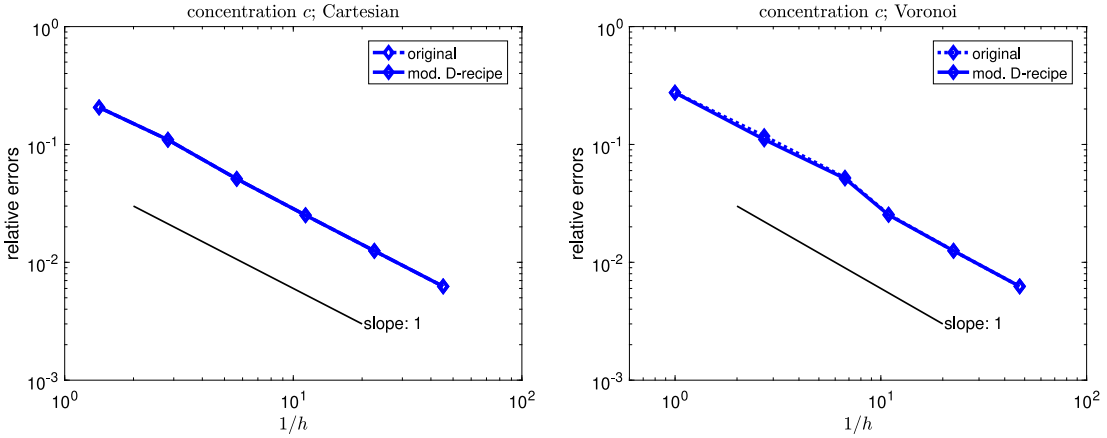

Fig. 4. Example 1. Relative L^2 errors for the concentration at the final time T on regular Cartesian meshes (left) and Voronoi meshes (right). The original stabilization (33) and the D-recipe stabilization (76) are employed.

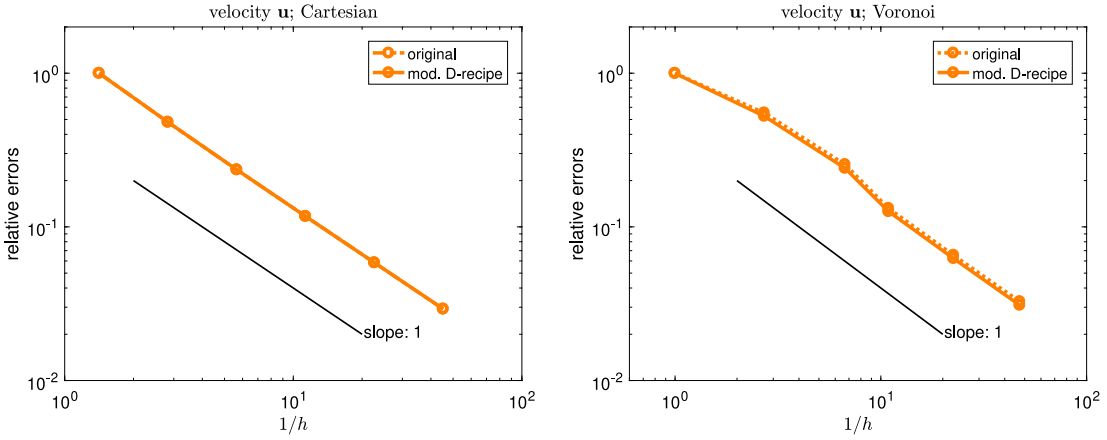

Fig. 5. Example 1. Relative L^2 errors for the velocity field at the final time T on regular Cartesian meshes (left) and Voronoi meshes (right). The original stabilization (33) and the D-recipe stabilization (76) are employed.

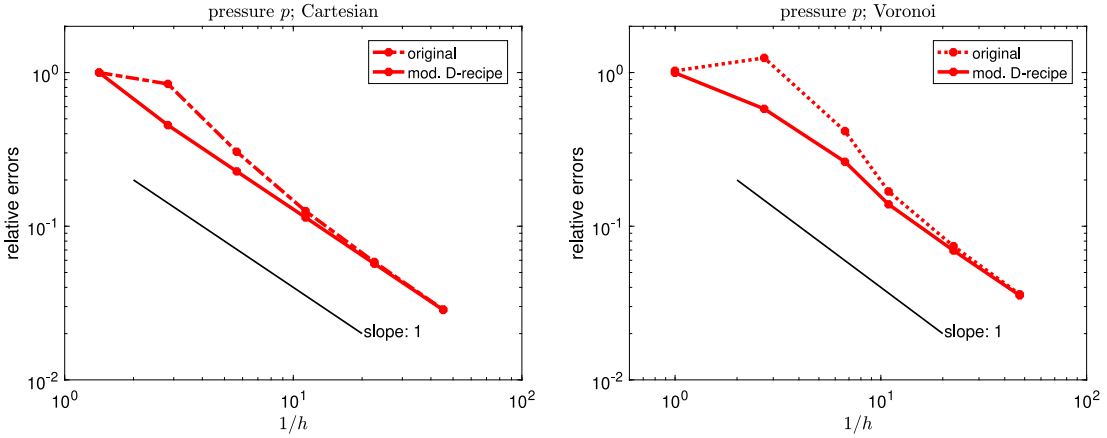

Fig. 6. Example 1. Relative L^2 errors for the pressure at the final time T on regular Cartesian meshes (left) and Voronoi meshes (right). The original stabilization (33) and the D-recipe stabilization (76) are employed.

with $R = 5$. The difference in error was only at the fourth meaningful digit; we do not plot the graphs since these would completely overlap the ones of the original method.

Example 2. The aim of the present test is to exploit the VEM capability of using locally refined meshes. We consider the generalized equation (74) with the same problem parameters of Example 1. The boundary conditions and the functions f and g are taken in accordance with the analytical solutions

$$\begin{aligned} c(x, y, t) &= t^2 \left[1 - e^{-100(x^2+y^2)}\right] \\ \boldsymbol{u}(x, y, t) &= 200t^2 \begin{pmatrix} xe^{-100(x^2+y^2)} \\ ye^{-100(x^2+y^2)} \end{pmatrix} \\ p(x, y, t) &= -\frac{1}{2}c^2 - 2c + \eta_1 t^4 + \eta_2 t^2, \end{aligned} \tag{78}$$

where the constants η_1, η_2 are such that $p(\cdot, t) \in L^2_0(\Omega)$ for all $t \in (0, T)$.

Note that the analytical solutions are such that they present a corner layer centered in $(0, 0)$ for all $t \in (0, T)$. The idea is to exploit this feature of the analytical solutions and the possibility of the VEM technology of using locally refined meshes.

We consider the family of locally refined meshes defined starting by a 4×4 uniform Cartesian mesh on $[0, 1]^2$, where the lower left square (corresponding to $[0.25, 0.25]^2$) is refined into 4×4, 8×8, 16×16, and 32×32 uniform Cartesian meshes (see Fig. 7 for a sample of the adopted meshes).

In Fig. 7, we exhibit the relative L^2 errors (against the total number of degrees of freedom) obtained with the locally refined meshes and time step τ chosen proportionally to the diameter of the refined squares. In order to assess the performance of the VEM technology on locally refined meshes, we also plot the results obtained with the family of 4×4, 8×8, 16×16, and 32×32 uniform Cartesian meshes on the whole domain $[0, 1]^2$. In this test, we use the diagonal stabilization (cf. (76)).

Notice that, excluding the concentrations where the errors appear to be dominated by the time discretization, for the velocity and the pressure, we obtain better results with the locally refined meshes. Although, due to the nature of the exact solution, these results are in accordance with the expectations, this test also serves the purpose of showing the robustness of the proposed VEM scheme with respect to elements with many hanging nodes (the last local refined mesh has 31 hanging nodes) which does not seem to deteriorate the accuracy of the scheme. Therefore, this kind of efficient refinement is indeed a viable choice for the proposed technology. Another classical situation in which flexible meshing would be useful is in the presence of jumping material data in accordance with complicated patterns/inclusions.

Example 3. Next, we investigate the behavior of the method for Test 1 and Test 2 in [32,52].

The problem is given in the form (1) with boundary conditions (4) and initial condition (5) over the spatial domain $\Omega = (0, 1000)^2$ ft^2. Moreover, $T = 3600$ days and $\tau = 36$ days. At the upper right corner, i.e. at $[1000, 1000]$, fluid with concentration $\widehat{c} = 1.0$ is injected with rate $q^+ = 30$ ft^2/day, whereas at the lower left corner, i.e. at $[0, 0]$, material is absorbed with rate $q^- = 30$ ft^2/day. Both wells are henceforth treated as Dirac masses, which is admissible at the discrete level since the discrete functions are piecewise regular (which can be interpreted as an approximation of the Dirac delta by a localized function with support within the corner element and unitary integral). Furthermore, the following choices for the parameters are picked: $\phi = 0.1$, $d_\ell = 50$, $d_t = 5$, $c_0 = 0$, $\boldsymbol{\gamma}(c) = 0$, and $a(c) = 80(1 + (M^{\frac{1}{4}} - 1)c)^4$, where

$$\text{Test A} : d_m = 10, M = 1; \qquad \text{Test B} : d_m = 0, M = 41.$$

Whereas $a(c)$ is constant for Test A, it changes rapidly across the fluid interface for Test B (which is in fact not covered by the theoretical analysis since $d_m = 0$, but is interesting to study numerically) resulting in a much faster propagation of the fluid concentration front along the diagonal direction ($d_\ell \gg d_t$). This effect is known as *macroscopic fingering phenomenon* [70].

For this example, we used a regular 25×25 Cartesian mesh and we employed the more sophisticated stabilization in (76). Since Test B is highly convection-dominated, pure application of our method leads to local disturbances

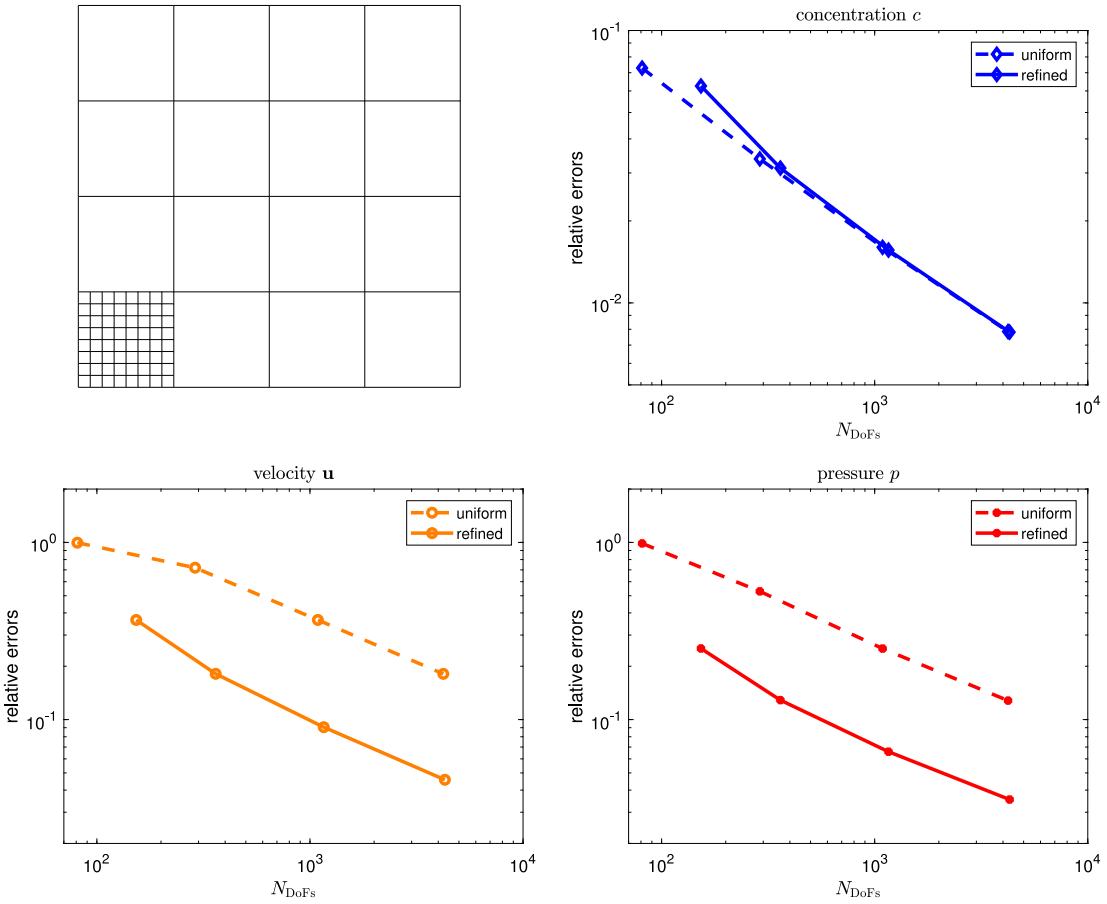

Fig. 7. Example 2. Sample of the adopted refined meshes (upper left). Relative L^2 errors for the concentration (upper right), relative L^2 errors for the velocity field (lower left) and relative L^2 errors for the pressure (lower right) at the final time T on regular Cartesian meshes and on corner refined meshes.

in the form of *overshoots* and *undershoots* of the numerical solution for the concentration, typical in the context of convection-dominated problem. To this purpose, for this test case, we employ the flux-corrected transport (FCT) algorithm with linearization [53,71]. The FCT scheme with linearization for convection-dominated flow problems operates in two steps: (1) advance the solution in time by a low-order overly diffusive scheme to suppress spurious oscillations, (2) correct the solution using (linear) antidiffusive fluxes. In that way the computed solution does not show spurious oscillations and layers are not smeared.

Due to the fact that no analytical solutions are available for Test A and Test B, we plot the numerical solutions (and the corresponding contour plots) for the concentration after 3 and 10 years. These times correspond to $n = 30$ and $n = 100$, respectively. For visualization of the results, since the numerical solution is virtual, but the nodal values are known, we simply add, inside each square, the barycenter with associated mean value of the nodal values, then create a triangulation based upon these points, and finally interpolate the function values linearly inside each triangle. In Figs. 8 and 9, the results for Test A are portrayed, and in Figs. 10 and 11, those for Test B. The results are similar to those obtained in [32,52].

6. Conclusions

We presented a virtual element method for the miscible displacement of one incompressible fluid by another in a reservoir, following a meaningful model instrumental to applications such as oil recovery and environmental pollution. We combined our VEM discretization in space with a cheap but effective discretization scheme in time.

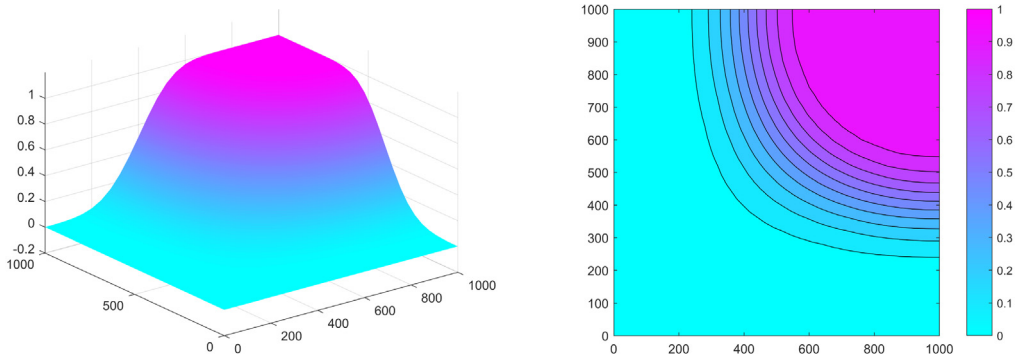

Fig. 8. Example 3. Numerical solution for the concentration (left) and contour plot (right) after 3 years in Test A.

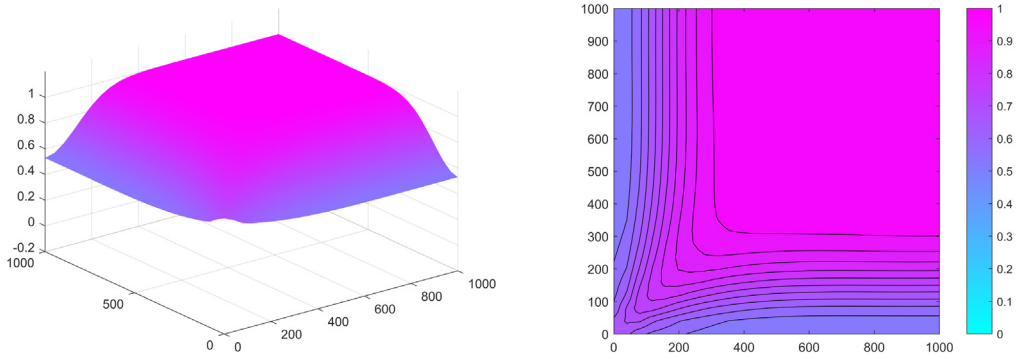

Fig. 9. Example 3. Numerical solution for the concentration (left) and contour plot (right) after 10 years in Test A.

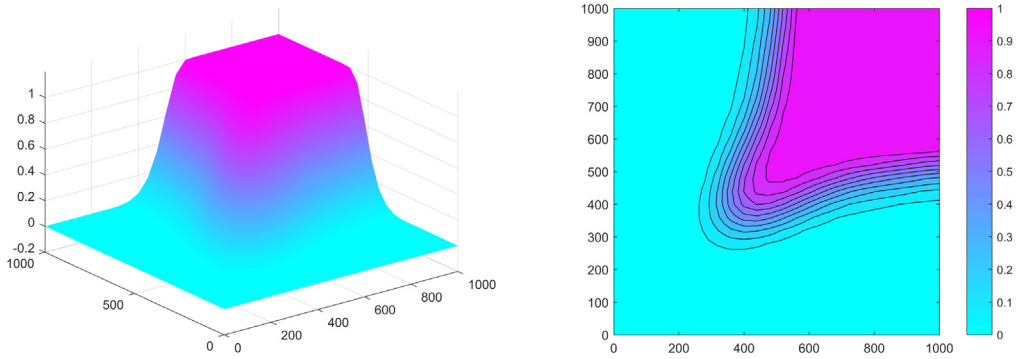

Fig. 10. Example 3. Numerical solution for the concentration (left) and contour plot (right) after 3 years in Test B.

After proposing the method, we developed an error analysis under the assumption of a regular solution, yielding a theoretical backbone to the scheme. No time step size condition was needed in the analysis.

We firstly tested the proposed method on an academic example, thus validating also numerically the convergence properties of the scheme and assessing some additional practical aspects (such as the possibility of using locally refined meshes that exploit the VEM flexibility). Afterwards, we considered a more realistic test case in order to have a qualitative comparison with the expected benchmark solution from the literature, in which we also introduced a modification in the method in order to deal with issues related to the convective nature of the problem. Although all the above developments are focused on the 2D case, we included an Appendix describing the extension to 3D problems.

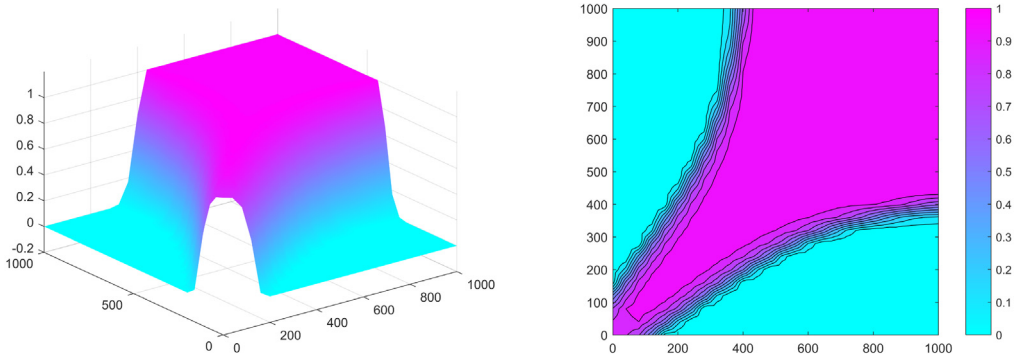

Fig. 11. Example 3. Numerical solution for the concentration (left) and contour plot (right) after 10 years in Test B.

From the presented theoretical and numerical studies, we believe that the VEM is promising and has the possibility to become, after further developments, a competitive scheme for complex flow problems. The added value, with respect to many competitors, is the possibility to easily handle arbitrarily shaped polytopal grids, which could be a critical point in geophysical real-life flow problems (that are well known to pose severe constraints to the creation of the computational meshes and easily give rise to distorted and badly shaped grid elements). The next step in the development of our VEM methodology will be to tackle more complex problems in two and three space dimensions, where we can really test the advantages of the proposed formulation. This includes, for instance, to solve problems with complex material data, as it happens in reservoir/basin simulation, and discrete fracture networks coupled with a diffusive matrix. Testing these cases, in collaboration with experts in the field, will be the scope of future communications.

Declaration of competing interest

The authors declare that they have no known competing financial interests or personal relationships that could have appeared to influence the work reported in this paper.

Acknowledgments

The first (L.B.d.V.) and last (G.V.) authors were partially supported by the European Research Council through the H2020 Consolidator Grant (Grant No. 681162) CAVE, Challenges and Advancements in Virtual Elements. This support is gratefully acknowledged. The second author (A.P.) has been funded by the Austrian Science Fund (FWF) through the project P 29197-N32, and by the Doctoral Program (DK), Austria through the FWF Project W1245.

Appendix. The three-dimensional case

The aim of this section is to present a brief discussion about the extension of the proposed method to the three-dimensional case, taking advantage of the ideas developed for the two-dimensional case combined with the construction in [3,62].

From now on, we will denote with P a general polyhedron having ℓ_V vertices V, ℓ_e edges e and ℓ_f faces f. Moreover, for each polyhedron P and each face f of P, we denote with $\boldsymbol{n}_P^f$ the unit outward normal vector to f, and with h_P, $|P|$, and $|f|$ the diameter of P, the volume of P, and the area of f, respectively.

Let $\mathcal{T}_h$ be a discretization of Ω into polyhedra P with $h := \max_{P\in\mathcal{T}_h} h_P$. For a given element $P \in \mathcal{T}_h$, $\mathcal{F}^P$ and $\mathcal{E}^P$ denote the sets of faces and edges belonging to P.

On each polyhedron $P \in \mathcal{T}_h$, the local velocity and pressure VE spaces are defined by

$$\begin{aligned}\boldsymbol{V}_h(P) := \{&\boldsymbol{v} \in H(\mathrm{div};P)\cap H(\mathbf{curl};P) : \ \boldsymbol{v}\cdot\boldsymbol{n}^f_{P|_f} \in \mathbb{P}_k(f)\,\forall f\in\partial P,\\ &\mathrm{div}\,\boldsymbol{v}\in\mathbb{P}_k(P),\ \mathbf{curl}\,\boldsymbol{v}\in\mathcal{R}_{k-1}(P)\}\\ Q_h(P) := \{&q\in L^2(P) : \ q\in\mathbb{P}_k(P)\},\end{aligned}$$

where $\mathcal{R}_{k-1}(P) := \mathbf{curl}\,([\mathbb{P}_k(P)])^3$. The local concentration space is defined (recursively) as

$$Z_h^{3D}(P) := \{z \in H^1(P) : z_{|\partial P} \in C^0(\partial P),\ z_{|f} \in Z_h(f)\,\forall f \in \mathcal{F}^P,\ \Delta z \in \mathbb{P}_{k+1}(P),$$
$$\int_P z\, p_k\,\mathrm{d}x = \int_P (\Pi_{k+1}^{\nabla,P} z)\, p_k\,\mathrm{d}x \quad \forall p_k \in \mathbb{P}_{k+1}/\mathbb{P}_{k-1}(P)\}.$$

We here summarize the main properties of the 3D spaces $\boldsymbol{V}_h(P)$, $Q_h(P)$ and $Z_h^{3D}(P)$ (we refer [3,62] for a deeper analysis).

- **Dimensions.** The dimensions of the 3D spaces $\boldsymbol{V}_h(P)$, $Q_h(P)$ and $Z_h^{3D}(P)$ are

$$\dim \boldsymbol{V}_h(P) = \ell_f \frac{(k+1)(k+2)}{2} + \frac{k(k+2)(k+3)}{2}$$
$$\dim Q_h(P) = \frac{(k+1)(k+2)(k+3)}{6}$$
$$\dim Z_h^{3D}(P) = \ell_V + \ell_e\, k + \ell_f \frac{k(k+1)}{2} + \frac{k(k+1)(k+2)}{6}.$$

- **Degrees of freedom (DoFs).** The following linear operators constitute a set of DoFs:
  - for $\boldsymbol{V}_h(P)$, a set of degrees of freedom $\{\mathrm{dof}_j^{\boldsymbol{V}_h(P)}\}_{j=1}^{\dim \boldsymbol{V}_h(P)}$ is defined by

$$\begin{aligned}
&1.\quad \frac{1}{|f|}\int_f \boldsymbol{v}\cdot\boldsymbol{n}_P^f\, p_k\,\mathrm{d}f \qquad \forall p_k \in \mathbb{P}_k(f) \quad \forall f \in \mathcal{F}^P\\
&2.\quad \frac{h_P}{|P|}\int_P (\mathrm{div}\,\boldsymbol{v})\, p_k\,\mathrm{d}x \qquad \forall p_k \in \mathbb{P}_k(P)/\mathbb{R}\\
&3.\quad \frac{1}{|P|}\int_K \boldsymbol{v}\cdot(\boldsymbol{x}\wedge\boldsymbol{p}_{k-1})\,\mathrm{d}x \qquad \forall \boldsymbol{p}_{k-1} \in [\mathbb{P}_{k-1}(P)]^3,
\end{aligned} \tag{79}$$

    with $\boldsymbol{x} := (x_1, x_2, x_3)^T$, where we assume the coordinates to be centered at the barycenter of the element;
  - for $Q_h(P)$, we consider $\{\mathrm{dof}_j^{Q_h(P)}\}_{j=1}^{\dim Q_h(P)}$ with

$$\frac{1}{|P|}\int_P q\, p_k\,\mathrm{d}x \qquad \forall p_k \in \mathbb{P}_k(P); \tag{80}$$

  - for $Z_h^{3D}(P)$, we take $\{\mathrm{dof}_j^{Z_h^{3D}(P)}\}_{j=1}^{\dim Z_h^{3D}(P)}$ with

$$\begin{aligned}
&1.\quad \text{pointwise values at the vertices: } z(\boldsymbol{v})\\
&2.\quad \text{on each edge } e \in \mathcal{E}^P, \text{ the values of } z \text{ at the } k \text{ internal Gauß–Lobatto points}\\
&3.\quad \frac{1}{|f|}\int_f z\, q_{k-1}\,\mathrm{d}f \qquad \forall q_{k-1} \in \mathbb{P}_{k-1}(f) \quad \forall f \in \mathcal{F}^P\\
&4.\quad \frac{1}{|P|}\int_P z\, q_{k-1}\,\mathrm{d}x \qquad \forall q_{k-1} \in \mathbb{P}_{k-1}(P).
\end{aligned} \tag{81}$$

- **Projections.** The DoFs allow us to exactly compute the polynomial projections

$$\Pi_{k+1}^{\nabla,P}: Z_h^{3D}(P) \to \mathbb{P}_{k-1}(P), \qquad \Pi_{k+1}^{0,P}: Z_h^{3D}(P) \to \mathbb{P}_{k-1}(P),$$
$$\boldsymbol{\Pi}_{\boldsymbol{k}}^{\boldsymbol{0},\boldsymbol{P}}: \boldsymbol{V}_h(P) \to [\mathbb{P}_k(P)]^3, \qquad \boldsymbol{\Pi}_{\boldsymbol{k}}^{\boldsymbol{0},\boldsymbol{P}}: \nabla Z_h^{3D}(P) \to [\mathbb{P}_k(P)]^3.$$

Once the above spaces with associated DoFs have been selected, the method design in the 3D setting follows the lines of Sections 3.3 and 3.4 verbatim. In particular, the forms $\mathcal{M}_h$, Θ_h, $\mathcal{D}_h$, and $\mathcal{A}_h$ in (24) follow the same constructions dictated in (26), (27), (29), and (31), respectively, where, in accordance with Remark 3.3, in order to get the 3D counterpart of the stability estimates (32), we take the following scaled stabilizations corresponding to

the degrees of freedom:

$$S^P_{\mathcal{M}}(c_h, z_h) = |P| \sum_{j=1}^{\dim Z_h^{3D}(P)} \mathrm{dof}_j^{Z_h^{3D}(P)}(c_h)\, \mathrm{dof}_j^{Z_h^{3D}(P)}(z_h)$$

$$S^P_{D}(c_h, z_h) = h_P \sum_{j=1}^{\dim Z_h^{3D}(P)} \mathrm{dof}_j^{Z_h^{3D}(P)}(c_h)\, \mathrm{dof}_j^{Z_h^{3D}(P)}(z_h)$$

$$S^P_{\mathcal{A}}(\boldsymbol{u}_h, \boldsymbol{v}_h) = |P| \sum_{j=1}^{\dim \boldsymbol{V}_h(P)} \mathrm{dof}_j^{\boldsymbol{V}_h(P)}(\boldsymbol{u}_h)\, \mathrm{dof}_j^{\boldsymbol{V}_h(P)}(\boldsymbol{v}_h).$$

Extending the theoretical results of the present paper to the 3D setting would not be particularly complicated. Essentially, the same path can be followed, combined with the approximation estimates (and the de Rham complex properties) of the above 3D virtual spaces, described in [62]. Delving into the details of such proofs is beyond the scope of the present paper.

References

[1] L. Beirão da Veiga, F. Brezzi, A. Cangiani, G. Manzini, L.D. Marini, A. Russo, Basic principles of virtual element methods, Math. Models Methods Appl. Sci. 23 (1) (2013) 199–214.

[2] L. Beirão da Veiga, F. Brezzi, L.D. Marini, A. Russo, The Hitchhiker's guide to the virtual element method, Math. Models Methods Appl. Sci. 24 (8) (2014) 1541–1573.

[3] L. Beirão da Veiga, F. Dassi, A. Russo, High-order virtual element method on polyhedral meshes, Comput. Math. Appl. 74 (2017) 1110–1122.

[4] F. Brezzi, L.D. Marini, Virtual element method for plate bending problems, Comput. Methods Appl. Mech. Engrg. 253 (2013) 455–462.

[5] P.F. Antonietti, L. Beirão da Veiga, S. Scacchi, M. Verani, A $\mathcal{C}^1$ virtual element method for the Cahn–Hilliard equation with polygonal meshes, SIAM J. Numer. Anal. 54 (1) (2016) 34–56.

[6] A. Cangiani, G. Manzini, O.J. Sutton, Conforming and nonconforming virtual element methods for elliptic problems, IMA J. Numer. Anal. 37 (2017) 1317–1354.

[7] S. Bertoluzza, M. Pennacchio, D. Prada, BDDC and FETI-DP for the virtual element method, Calcolo 54 (4) (2017) 1565–1593.

[8] L. Beirão da Veiga, C. Lovadina, G. Vacca, Virtual elements for the Navier-Stokes problem on polygonal meshes, SIAM J. Numer. Anal. 56 (3) (2018) 1210–1242.

[9] E. Cáceres, G.N. Gatica, F.A. Sequeira, A mixed virtual element method for quasi-Newtonian Stokes flows, SIAM J. Numer. Anal. 56 (1) (2018) 317–343.

[10] L. Beirão da Veiga, F. Brezzi, F. Dassi, L.D. Marini, A. Russo, Lowest order virtual element approximation of magnetostatic problems, Comput. Methods Appl. Mech. Engrg. 332 (2018) 343–362.

[11] S. Berrone, A. Borio, G. Manzini, SUPG stabilization for the nonconforming virtual element method for advection-diffusion-reaction equations, Comput. Methods Appl. Mech. Engrg. 340 (2018) 500–529.

[12] D. Mora, I. Velásquez, A virtual element method for the transmission eigenvalue problem, Math. Models Methods Appl. Sci. 28 (14) (2018) 2803–2831.

[13] L. Beirão da Veiga, A. Russo, G. Vacca, The virtual element method with curved edges, ESAIM Math. Model. Numer. Anal. 53 (2) (2019) 375–404.

[14] L. Mascotto, I. Perugia, A. Pichler, A nonconforming Trefftz virtual element method for the Helmholtz problem: numerical aspects, Comput. Methods Appl. Mech. Engrg. 347 (2019) 445–476.

[15] A. Hussein, F. Aldakheel, B. Hudobivnik, P. Wriggers, P. Guidault, O. Allix, A computational framework for brittle crack-propagation based on efficient virtual element method, Finite Elem. Anal. Des. 159 (2019) 15–32.

[16] H. Chi, A. Pereira, G. Paulino, I. Menezes, Virtual element method (VEM)-based topology optimization: an integrated framework, Struct. Multidiscip. Optim. (2019) http://dx.doi.org/10.1007/s00158-019-02268-w.

[17] L. Beirão da Veiga, F. Brezzi, L.D. Marini, A. Russo, Virtual element method for general second-order elliptic problems on polygonal meshes, Math. Models Methods Appl. Sci. 26 (4) (2016) 729–750.

[18] L. Beirão da Veiga, F. Brezzi, L.D. Marini, A. Russo, Mixed virtual element methods for general second order elliptic problems on polygonal meshes, ESAIM Math. Model. Numer. Anal. 50 (3) (2016) 727–747.

[19] A. Cangiani, G. Manzini, A. Russo, N. Sukumar, Hourglass stabilization and the virtual element method, Internat. J. Numer. Methods Engrg. 102 (3–4) (2015) 404–436.

[20] G. Vacca, L. Beirão da Veiga, Virtual element methods for parabolic problems on polygonal meshes, Numer. Methods Partial Differential Equations 31 (6) (2015) 2110–2134.

[21] M.F. Benedetto, S. Berrone, A. Borio, S. Pieraccini, S. Scialò, Order preserving SUPG stabilization for the virtual element formulation of advection-diffusion problems, Comput. Methods Appl. Mech. Engrg. 311 (2016).

[22] P.F. Antonietti, L. Formaggia, A. Scotti, M. Verani, N. Verzott, Mimetic finite difference approximation of flows in fractured porous media, ESAIM Math. Model. Numer. Anal. 50 (3) (2016) 809–832.

[23] L. Formaggia, A. Scotti, F. Sottocasa, Analysis of a mimetic finite difference approximation of flows in fractured porous media, ESAIM Math. Model. Numer. Anal. 52 (2) (2018) 595–630.
[24] M.F. Benedetto, S. Berrone, S. Pieraccini, S. Scialò, The virtual element method for discrete fracture network simulations, Comput. Methods Appl. Mech. Engrg. 280 (2014) 135–156.
[25] M.F. Benedetto, S. Berrone, A. Borio, S. Pieraccini, S. Scialò, A hybrid mortar virtual element method for discrete fracture network simulations, J. Comput. Phys. 306 (2016) 148–166.
[26] S. Berrone, A. Borio, S. Scialò, A posteriori error estimate for a PDE-constrained optimization formulation for the flow in DFNs, SIAM J. Numer. Anal. 54 (1) (2016) 242–261.
[27] S. Berrone, A. Borio, C. Fidelibus, S. Pieraccini, S. Scialò, F. Vicini, Advanced computation of steady-state fluid flow in discrete fracture-matrix models: FEM-BEM and VEM-VEM fracture-block coupling, GEM Int. J. Geomath. 9 (2) (2018) 377–399.
[28] A. Fumagalli, E. Keilegavlen, Dual virtual element method for discrete fractures networks, SIAM J. Sci. Comput. 40 (1) (2018) B228–B258.
[29] T.F. Russell, M.F. Wheeler, Finite element and finite difference methods for continuous flows in porous media, in: The Mathematics of Reservoir Simulation, SIAM, 1983, pp. 35–106.
[30] D.W. Peaceman, Fundamentals of Numerical Reservoir Simulation, Vol. 6, Elsevier, 2000.
[31] J. Douglas Jr., R.E. Ewing, The approximation of the pressure by a mixed method in the simulation of miscible displacement, RAIRO Anal. Numer. 17 (1) (1983) 17–33.
[32] C. Chainais-Hillairet, J. Droniou, Convergence analysis of a mixed finite volume scheme for an elliptic–parabolic system modeling miscible fluid flows in porous media, SIAM J. Numer. Anal. 45 (5) (2007) 2228–2258.
[33] J. Droniou, R. Eymard, A. Prignet, K.S. Talbot, Unified convergence analysis of numerical schemes for a miscible displacement problem, Found. Comput. Math. 19 (2) (2019) 333–374.
[34] M. Berardi, F. Difonzo, L. Lopez, A mixed MoL-TMol for the numerical solution of the 2D Richards' equation in layered soils, Comput. Math. Appl. 79 (2020) 1990–2001.
[35] M. Berardi, F. Difonzo, F. Notarnicola, M. Vurro, A transversal method of lines for the numerical modeling of vertical infiltration into the vadose zone, Appl. Numer. Math. 135 (2019) 264–275.
[36] R.E. Ewing, M.F. Wheeler, Galerkin methods for miscible displacement problems in porous media, SIAM J. Numer. Anal. 17 (3) (1980) 351–365.
[37] R.E. Ewing, M.F. Wheeler, Galerkin methods for miscible displacement problems with point sources and sinks—unit mobility ratio case, in: Mathematical Methods in Energy Research (Laramie, Wyo. 1982/1983), SIAM, Philadelphia, PA, 1984, pp. 40–58.
[38] M.F. Wheeler, B.L. Darlow, Interior penalty Galerkin procedures for miscible displacement problems in porous media, in: Computational Methods in Nonlinear Mechanics (Proc. Second Internat. Conf. Univ. Texas, Austin, Tex. 1979), North-Holland, Amsterdam, 1980, pp. 485–506.
[39] S. Bartels, M. Jensen, R. Müller, Discontinuous Galerkin finite element convergence for incompressible miscible displacement problems of low regularity, SIAM J. Numer. Anal. 47 (5) (2009) 3720–3743.
[40] B.M. Rivière, N.J. Walkington, Convergence of a discontinuous Galerkin method for the miscible displacement equation under low regularity, SIAM J. Numer. Anal. 49 (3) (2011) 1085–1110.
[41] J. Li, B. Riviere, N. Walkington, Convergence of a high order method in time and space for the miscible displacement equations, ESAIM Math. Model. Numer. Anal. 49 (4) (2015) 953–976.
[42] S. Sun, B. Riviére, M.F. Wheeler, A combined mixed finite element and discontinuous Galerkin method for miscible displacement problem in porous media, in: Recent Progress in Computational and Applied PDES, 2002, pp. 323–351.
[43] H. Guo, F. Yu, Y. Yang, Local discontinuous Galerkin method for incompressible miscible displacement problem in porous media, J. Sci. Comput. 71 (2017) 615–633.
[44] H. Wang, J. Zheng, F. Yu, H. Guo, Q. Zhang, Local discontinuous Galerkin method with implicit-explicit time marching for incompressible miscible displacement problem in porous media, J. Sci. Comput. 78 (2019) 1–28.
[45] B. Amaziane, M. El Ossmani, Convergence analysis of an approximation to miscible fluid flows in porous media by combining mixed finite element and finite volume methods, Numer. Methods Partial Differential Equations 24 (3) (2008) 799–832.
[46] C. Chainais-Hillairet, S. Krell, A. Mouton, Study of discrete duality finite volume schemes for the Peaceman model, SIAM J. Sci. Comput. 35 (6) (2013) A2928–A2952.
[47] F. Chave, D.A. Di Pietro, L. Formaggia, A hybrid high-order method for Darcy flows in fractured porous media, SIAM J. Sci. Comput. 40 (2) (2018) A1063–A1094.
[48] F. Chave, D.A. Di Pietro, L. Formaggia, A hybrid high-order method method for passive transport in fractured porous media, GEM Int. J. Geomath. 10 (1) (2019) 12.
[49] P.F. Antonietti, C. Facciola, A. Russo, M. Verani, Discontinuous Galerkin approximation of flows in fractured porous media on polytopic grids, SIAM J. Sci. Comput. 41 (1) (2019) A109–A138.
[50] F. Brezzi, R.S. Falk, L.D. Marini, Basic principles of mixed virtual element methods, ESAIM Math. Model. Numer. Anal. 48 (4) (2014) 1227–1240.
[51] H. Hu, Y. Fu, J. Zhou, Numerical solution of a miscible displacement problem with dispersion term using a two-grid mixed finite element approach, Numer. Algorithms 81 (3) (2019) 879–914.
[52] H. Wang, D. Liang, R.E. Ewing, S.L. Lyons, G. Qin, An approximation to miscible fluid flows in porous media with point sources and sinks by an Eulerian–Lagrangian localized adjoint method and mixed finite element methods, SIAM J. Sci. Comput. 22 (2) (2000) 561–581.
[53] D. Kuzmin, Explicit and implicit FEM-FCT algorithms with flux linearization, J. Comput. Phys. 228 (7) (2009) 2517–2534.

[54] V. John, E. Schmeyer, Finite element methods for time-dependent convection–diffusion-reaction equations with small diffusion, Comput. Methods Appl. Mech. Engrg. 198 (3–4) (2008) 475–494.
[55] H. Triebel, Interpolation Theory, Function Spaces, Differential Operators, North-Holland, 1978.
[56] X.B. Feng, On existence and uniqueness results for a coupled system modeling miscible displacement in porous media, J. Math. Anal. Appl. 194 (3) (1995) 883–910.
[57] Z. Chen, R. Ewing, Mathematical analysis for reservoir models, SIAM J. Math. Anal. 30 (2) (1999) 431–453.
[58] A. Quarteroni, A. Valli, Numerical Approximation of Partial Differential Equations, in: Springer Series in Computational Mathematics, vol. 23, Springer-Verlag, Berlin, 1994.
[59] L. Beirão da Veiga, C. Lovadina, A. Russo, Stability analysis for the virtual element method, Math. Models Methods Appl. Sci. 27 (13) (2017) 2557–2594.
[60] S.C. Brenner, Q. Guan, L.Y. Sung, Some estimates for virtual element methods, Comput. Methods Appl. Math. 17 (4) (2017) 553–574.
[61] S.C. Brenner, L.Y. Sung, Virtual element methods on meshes with small edges or faces, Math. Models Methods Appl. Sci. 28 (07) (2018) 1291–1336.
[62] L. Beirão da Veiga, F. Brezzi, L.D. Marini, A. Russo, $H(\mathrm{div})$ and $H(\mathrm{curl})$-conforming virtual element methods, Numer. Math. 133 (2) (2016) 303–332.
[63] B. Ahmad, A. Alsaedi, F. Brezzi, L.D. Marini, A. Russo, Equivalent projectors for virtual element methods, Comput. Math. Appl. 66 (3) (2013) 376–391.
[64] L. Beirão da Veiga, F. Brezzi, L.D. Marini, A. Russo, Virtual element method for general second-order elliptic problems on polygonal meshes, Math. Models Methods Appl. Sci. 26 (4) (2016) 729–750.
[65] S.C. Brenner, L.R. Scott, The Mathematical Theory of Finite Element Methods, third ed., in: Texts in Applied Mathematics, vol. 15, Springer-Verlag, New York, 2008.
[66] M. Braun, M. Golubitsky, Differential Equations and their Applications, Vol. 4, Springer, 1983.
[67] S.C. Brenner, Poincaré–Friedrichs inequalities for piecewise H^1 functions, SIAM J. Numer. Anal. 41 (1) (2003) 306–324.
[68] A. Cangiani, E.H. Georgoulis, T. Pryer, O.J. Sutton, A posteriori error estimates for the virtual element method, Numer. Math. 137 (2017) 857–893.
[69] V. Thomée, Galerkin Finite Element Methods for Parabolic Problems, Vol. 1054, Springer, 1984.
[70] R.E. Ewing, The Mathematics of Reservoir Simulation, SIAM, 1983.
[71] D. Kuzmin, M. Möller, Algebraic flux correction. I Scalar conservation laws, in: Flux-corrected Transport, Sci. Comput., Springer, Berlin, 2005, pp. 155–206.